



HAL
open science

Parameters and determinants of responses to selection in antibody libraries

Steven Schulz, Sébastien Boyer, Matteo Smerlak, Simona Cocco, Remi Monasson, Clément Nizak, Olivier Rivoire

► To cite this version:

Steven Schulz, Sébastien Boyer, Matteo Smerlak, Simona Cocco, Remi Monasson, et al.. Parameters and determinants of responses to selection in antibody libraries. 2020. hal-03190048v1

HAL Id: hal-03190048

<https://hal.science/hal-03190048v1>

Preprint submitted on 6 Nov 2020 (v1), last revised 6 Oct 2021 (v2)

HAL is a multi-disciplinary open access archive for the deposit and dissemination of scientific research documents, whether they are published or not. The documents may come from teaching and research institutions in France or abroad, or from public or private research centers.

L'archive ouverte pluridisciplinaire **HAL**, est destinée au dépôt et à la diffusion de documents scientifiques de niveau recherche, publiés ou non, émanant des établissements d'enseignement et de recherche français ou étrangers, des laboratoires publics ou privés.

Parameters and determinants of responses to selection in antibody libraries

Steven Schulz^a, Sébastien Boyer^b, Matteo Smerlak^c, Simona Cocco^d, Rémi Monasson^d, Clément Nizak^e,
and Olivier Rivoire^a

^a*Center for Interdisciplinary Research in Biology (CIRB), Collège de France, CNRS UMR 7241, INSERM U1050, PSL University, Paris, France*

^b*Département de biochimie, Faculté de Médecine, Université de Montréal, Montréal, Canada*

^c*Max Planck Institute for Mathematics in the Sciences, Leipzig, Germany*

^d*Laboratory of Physics of École Normale Supérieure, UMR 8023, CNRS & PSL University, Paris, France*

^e*Chimie Biologie Innovation, ESPCI Paris, CNRS, PSL University, Paris, France*

Abstract

Antibody repertoires contain binders to nearly any target antigen. The sequences of these antibodies differ mostly at few sites located on the surface of a scaffold that itself consists of much less varied amino acids. What is the impact of this scaffold on the response to selection of a repertoire? To gauge this impact, we carried out quantitative phage display experiments with three antibody libraries based on distinct scaffolds harboring the same diversity at randomized sites, which we selected for binding to four arbitrary targets. We first show that the response to selection of an antibody library is captured by a simple and measurable parameter with direct physical and information-theoretic interpretations. Second, we identify a major determinant of this parameter which is encoded in the scaffold, its degree of evolutionary maturation. Antibodies undergo an accelerated evolutionary process, called affinity maturation, to improve their affinity to a given target antigen as part of the adaptive immune response. We find that libraries of antibodies built around such matured scaffolds have a lower response to selection to other arbitrary targets than libraries built around naïve scaffolds of germline origin. Our results are a first step towards quantifying and controlling the evolutionary potential of biomolecules.

1. Introduction

1 The idea that evolution by natural selection is not only leading to adaptations but to a propensity
2 to adapt, or “evolvability”, has been repeatedly put forward [1, 2, 3]. As demonstrated by a number
3 of mathematical models, evolvability can indeed emerge from evolutionary dynamics without any direct
4 selection for it [4, 5, 6, 7]. Yet, theoretical insights have not translated into experimental assays for measuring
5 and controlling evolvability in actual biological systems. Biomolecules as RNAs and proteins are ideal
6 model systems for developing such assays as they are amenable to controlled experimental evolution [8]. For
7 proteins, in particular, several biophysical and structural features have been proposed to correlate with their
8 evolvability, most notably their thermal stability [9] and the modularity and polarity of their native fold [10].
9 A major limitation, however, is the absence of a measurable index of evolvability quantifying evolutionary
10 responses to compare to biophysical or structural quantities.

11 Here, we present results of quantitative selection experiments with antibodies that address this issue.
12 Antibodies are particularly well suited to devise and test new approaches to measure and control evolvability.
13 They conveniently span a large phenotypic diversity, specific binding to virtually any molecular target, by
14

15 means of a limited genotypic diversity. Most of the diversity of natural antibody repertoires is indeed
16 achieved by a few randomized loops that are displayed onto a structurally more conserved framework [11].
17 Further, well-established screening techniques are available for manipulating libraries of billions of diverse
18 antibodies [12]. More fundamentally, antibodies are subject to two evolutionary processes on two distinct
19 time scales: their frameworks evolve on the time scale of many generations of their host, as all other
20 genes, and both frameworks and loops also evolve on a much shorter time scale as part of the immune
21 response in the process of affinity maturation [13]. Importantly, affinity maturation-associated mutations
22 are somatic and the sequences of matured antibodies are not transmitted to subsequent generations.
23 Germline antibody frameworks, whose transmitted sequences are the starting point of affinity maturation,
24 are thus well positioned to be particularly evolvable, as evolving to increase their affinity to antigens is part
25 of their physiological role.

26 As a first step towards quantifying and controlling the evolvability of antibodies, we previously charac-
27 terized the response to selection of antibody libraries built around different structural scaffolds [14]. We took
28 for these scaffolds the frameworks of heavy chains (V_H) of natural antibodies, and built libraries by intro-
29 ducing all combinations of amino acids at four consecutive sites in their complementary determining region
30 (CDR3) loop, a part of their sequence known to determine their binding affinity and specificity [11]. Using
31 phage display [15], we selected sequences from these libraries for their ability to bind different molecular tar-
32 gets and inferred the relative enrichment, or selectivity, of different antibody sequences by high-throughput
33 sequencing [16]. Comparing experiments with libraries built on different scaffolds and selected against dif-
34 ferent targets led us to two conclusions. First, we quantified the variability of responses to selection of
35 different sequences within a library and found this variability to differ widely across experiments involving
36 different libraries and/or different targets. Second, we observed a hierarchy of selectivities between libraries,
37 with multiple sequences from one particular library dominating selections involving a mixture of different
38 libraries. These results raised two questions: (i) How to relate the hierarchies of selectivities between and
39 within libraries? (ii) How to rationalize the differences between scaffolds that are all homologous?

40 Here, we answer these two questions through the presentation of new data and new analyses. First,
41 we propose to characterize the hierarchies within and between libraries with two parameters for which we
42 provide interpretations from the three standpoints of physics, information theory and sequence content.
43 Second, we present new experimental results that identify the degree of maturation of an antibody scaffold
44 as a control parameter for its selective potential. The results are, to our knowledge, the first demonstration
45 based on quantifying the evolutionary responses to multiple selective pressures that long-term evolution has
46 endowed germline antibody frameworks with a special ability to respond to selection.

47 **2. Methods**

48 *2.1. Experimental design*

49 In the absence of mutations, the outcome of an evolutionary process is determined by the properties of
50 its initial population. In our experiments where antibodies are evolved in successive cycles of selection and
51 amplification, the critical property of a sequence x present in the initial population is its selectivity $s(x)$, the
52 factor by which it is enriched or depleted from one cycle to the next (see Box). Selection involves binding to
53 a target, which is varied between experiments. Experiments are designed for the selectivity $s(x)$ to reflect
54 the binding affinity of sequence x to this target (see Appendix 1.1). Inevitably, however, it can also depend

55 on affinity to non-target substrates and to sequence-dependent differences in amplification. Importantly,
56 while the details of these “biases” are contingent to the experimental approach, their presence is a generic
57 feature of any process of molecular evolution, including the natural process of antibody affinity maturation
58 of which the experiments mimic the first step, prior to the introduction of any mutation.

59 Each of our libraries consists of sequences with a common part, which we call a scaffold, and 4 positions
60 that are randomized to all $N = 20^4$ combinations, where 20 is the number of natural amino acids. The
61 mapping $x \mapsto s_{L,T}(x)$ from 4-position sequences x to selectivities thus depends both on the scaffold that
62 defines the library L and on the target T that defines the selective pressure. We are interested in properties
63 of the scaffold that favor large values of selectivities, where “large” is considered either relative to other
64 sequences within the same library (same scaffold) or relative to sequences from different libraries (different
65 scaffolds).

66 Our previous experiments involved 24 different libraries, each built on a different scaffold consisting of
67 a natural V_H fragment [14]. These fragments originate from the germline or the B cells of organisms of
68 various species. Scaffolds from the germline encode naïve antibodies which have not been subject to any
69 affinity maturation, while scaffolds from B cells encode matured antibodies which have evolved from naïve
70 antibodies to bind strongly to antigens encountered by the organisms. We previously performed experiments
71 where the initial population consisted either of a single library or a mixture of different libraries [14]. In
72 particular, in two experiments using very different targets (a neutral polymer and a DNA loop) we co-
73 selected all 24 libraries together. Strikingly, while only 2 of the 24 libraries were built on germline scaffolds,
74 the final population of one experiment was dominated by antibodies built on one of the two naïve scaffolds,
75 and the second by the other one. This suggested us that germline scaffolds may have an intrinsically higher
76 selective potential.

77 To investigate this hypothesis, we analyze here the selection against 4 different targets of 3 libraries with
78 varying degrees of maturation. The scaffolds of the 3 libraries originate from Human V_H fragments and
79 have evolved to different degrees as part of the immune response of patients infected by HIV (Fig. S1). The
80 first scaffold (Germ) is taken from the germline and has not undergone any maturation. The second scaffold
81 (Lim) has been subject to limited affinity maturation and differs from Germ, from which it originates, by
82 14 % of its amino acids. The third scaffold (Bnab) is a so-called broadly neutralizing antibody [17], which has
83 evolved over many years to recognize a conserved part of the HIV virus [18]; it also originates from Germ,
84 to which it differs by 34 % of its amino acids, and has evolved independently of Lim, to which it differs
85 by 38 %. The 3 libraries, which are built around these scaffolds by introducing all combinations of amino
86 acids at 4 positions of their CDR3 were part of the 24 libraries used in our previous experiments [14]. Here,
87 to systematically compare the selective potential of these libraries, we present experiments where they are
88 selected against four different targets, two DNA targets (DNA hairpins with a common stem but different
89 loops, denoted DNA1 and DNA2, Fig. S2) and two homologous protein targets (the fluorescent proteins
90 eGFP and mCherry, denoted prot1 and prot2), each unrelated to the HIV virus against which the Lim and
91 Bnab scaffolds had been matured.

92 *2.2. Parametrization*

93 To quantitatively compare the outcome of different experiments with different libraries and targets, we
94 introduce here two parameters, σ and μ , which respectively quantify intra and inter-library differences in
95 selectivities. These parameters derive from a statistical approach that considers only the distribution $P(s)$

96 of values that selectivities take across the different sequences of a library [19, 20, 21]. They correspond to
97 the assumption that this distribution is log-normal,

$$P(s) = \frac{1}{\sqrt{2\pi}\sigma s} \exp\left(-\frac{(\ln s - \mu)^2}{2\sigma^2}\right). \quad (1)$$

98 The parameter σ captures intra-library differences in response to selection while the parameter μ provides
99 the additional information required to describe inter-library differences.

100 The assumption that distributions of selectivities are log-normal has several justifications. First, it
101 empirically provides a good fit of the data, not only in our experiments as we show below, but in a number
102 of previous studies of antibody-antigen interactions [22] and protein-DNA interactions [23], including studies
103 that had access to the complete distribution $P(s)$ [23]. Second, log-normal distributions are stable upon
104 iteration of the evolutionary process: if two successive selections are performed so that $s = s_1 s_2$ with s_1 and
105 s_2 independently described by log-normal distributions with parameters (σ_1, μ_1) and (σ_2, μ_2) , s also follows a
106 log-normal distribution with parameters $\sigma = (\sigma_1^2 + \sigma_2^2)^{1/2}$ and $\mu = \ln[(\sigma_1^{-2} e^{\mu_1} + \sigma_2^{-2} e^{\mu_2})/\sigma^{-2}]$; more generally,
107 log-normal distributions are attractors of evolutionary dynamics [24]. Third, log-normal distributions are
108 physically justified from the simplest model of interaction, an additive model where the interaction energy
109 between sequence $x = (x_1, \dots, x_\ell)$ of length ℓ and its target takes the form $E(x) = \sum_{i=1}^{\ell} \epsilon_i(x_i)$ with
110 contributions $\epsilon_i(x_i)$ from each position i and amino acid x_i , and thus its selectivity $s(x) \simeq e^{-E(x)/k_B T}$,
111 where T is the temperature and k_B the Boltzmann constant (Appendix 1.1). At thermal equilibrium and
112 for sufficiently large ℓ , a log-normal distribution of the affinities is then expected with $\mu \sim -\ell\langle\epsilon\rangle/k_B T$ and
113 $\sigma \sim \ell^{1/2}(\langle\epsilon^2\rangle - \langle\epsilon\rangle^2)^{1/2}/k_B T$, where $\langle\epsilon\rangle$ and $\langle\epsilon^2\rangle - \langle\epsilon\rangle^2$ are respectively the mean and variance of the values
114 of binding energies per position $\epsilon_i(x_i)$.

115 2.3. Inference of parameters

116 Selectivities are measured as relative enrichments of sequences in two successive rounds of selection. We
117 obtain the parameters σ and μ by fitting the values with truncated log-normal distributions (Fig. 1A and
118 Appendix 3.3). This inference is complicated by two factors: only the upper tail of the distribution of selec-
119 tivities is sampled in the experiments and enrichments provide selectivities only up to a multiplicative factor
120 (see Box). While the parameter σ is independent of this multiplicative factor, comparing the parameters μ
121 between libraries requires performing selections where different libraries are mixed in the initial population.
122 To refine and validate our inference, we also performed selection experiments where we mixed a very small
123 number of random and top selectivity sequences (Fig. 1B): as the random sequences typically reflect the
124 mode of the distributions, (the most likely selectivity value), these experiments provide an independent
125 estimation of μ that we can profitably use (see details in Appendix 3.3).

126 The values of σ and μ that we infer for the 3 libraries Germ, Lim and Bnab when selected against each
127 of the 4 targets DNA1, DNA2, prot1 and prot2 are presented in Fig. 2A. We validated the quality of the
128 fits by probability-probability and quantile-quantile plots (Figs. S16-S18). We also assessed the robustness
129 of the inference by comparing replicate experiments (Figs. S16-S22), and comparing experiments where a
130 library is selected either alone or in mixture with the other two (Fig. S19). Finally, we verified that the
131 results are unchanged whether selectivities are measured from enrichments between the 2nd and 3rd cycles,
132 or the 3rd and 4th ones (Figs. S20-S21).

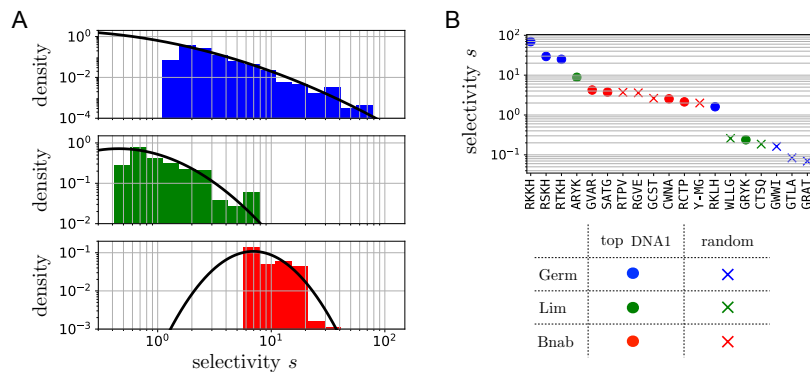


Figure 1: Fitting empirical distributions of selectivities with log-normal distributions. **A.** The selection of a library L against a target T provides the selectivities of the sequences in L that have top selectivity against T . Here, the histograms show the selectivities obtained from experiments where the Germ (in blue), Lim (in green) and Bnab (in red) libraries were selected against the DNA1 target. The black line is the best fit to a log-normal distribution. **B.** To locate precisely the mode of the distributions, we performed experiments where the initial population consists in a mixture of very few top (dots) and random (crosses) sequences. Top sequences are identified from A based on the largest selectivities against the target. Random sequences, on the other hand, are picked at random in the libraries and are expected to have typical selectivities located at the maxima of the black curves in A. Taken together, the results indicate that when selected against the DNA1 target, the Germ library has the highest σ and the Bnab library the highest μ . Similar results are obtained for selections against other targets (Fig. S8 and Table 1).

133 3. Results

134 3.1. Intra-library hierarchy

135 The hierarchy of selectivities within a library is quantified by the parameter σ : a small σ indicates that
 136 all sequences in the library are equally selected while a large σ indicates that the response to selection
 137 varies widely between sequences in the library. When comparing the $\sigma_{L,T}$ inferred from the selections of
 138 the 3 libraries L against each of the 4 targets T , a remarkable pattern emerges: the more a scaffold is
 139 matured, the smaller is σ , $\sigma_{\text{Germ},T} > \sigma_{\text{Lim},T} \geq \sigma_{\text{Bnab},T}$ for all targets T , and even $\min_T(\sigma_{\text{Germ},T}) >$
 140 $\max_T(\sigma_{\text{Lim},T}, \sigma_{\text{Bnab},T})$ (Fig. 2A). Statistically, if considering the inequalities to be strict, the experiments
 141 to be independent and any result to be *a priori* equally likely, the probability of this finding is only $p =$
 142 $(3!)^{-4} \simeq 7.10^{-4}$.

143 Examining sequence logos shows that although selections of the Germ library are characterized by a
 144 similarly high value of σ for the 4 targets, the sequences that are selected against each target are different
 145 (Fig. 2B-C). The amino acids found to be enriched are consistent with the nature of the targets: selections
 146 against the DNA targets are dominated by positively charged amino acids (letters in blue) and selections
 147 against the two protein targets, which are close homologs, are dominated by similar amino acid motifs.

148 In contrast, sequences logos for the Bnab library show motifs that are less dependent on the target
 149 (Fig. 2B and Fig. S10). This observation is rationalized by an experiment where only the amplification
 150 step is performed, in the absence of any selection for binding. Sequence-specific amplification biases are
 151 then revealed, with sequence motifs that are similar to those observed when selection for binding is present
 152 (Fig. S10). With protein targets at least, the motifs are nevertheless sufficiently different to infer that
 153 selection for binding to the target contributes significantly to the selectivities (see also Fig. S6). Target-
 154 specific selection for binding, which is dominating the top selectivities in the Germ library (Fig. S11), is
 155 thus of the same order of magnitude as amplification biases for the top selectivities in the Bnab library.

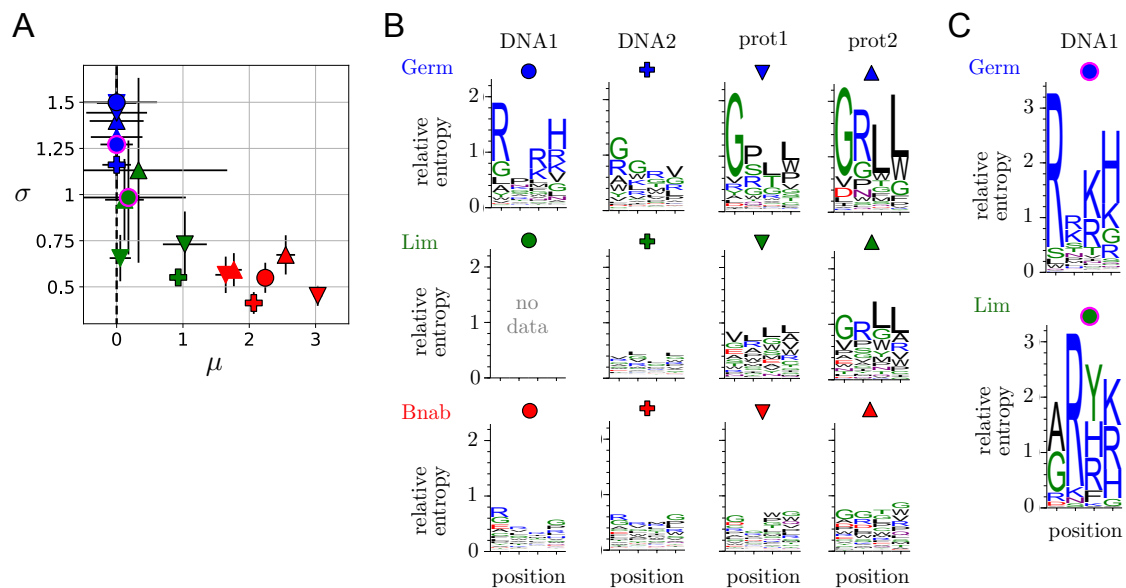


Figure 2: Comparing selections of libraries built on scaffolds with different degrees of maturation – **A**. Parameters (μ, σ) of the distributions of selectivities for our 3 libraries selected against 4 targets. The color of the symbols indicates the library (Germ, Lim or Bnab) and its shape the target (DNA1, DNA2, prot1 or prot2) with the conventions defined in B. Symbols with a black or no contour indicate results from replicate experiments where the 3 libraries are mixed in the initial population, and symbols with a magenta contour where a library is screened in isolation. $\mu_{\text{Germ}, T}$ is conventionally set to $\mu_{\text{Germ}, T} = 0$ for all targets T (Appendix 3.4). μ is generally more challenging to infer than σ and it shows here more variations across replicate experiments. **B**. Sequence logos for $\tilde{s}_i(a)$, which represent the contribution of the different amino acids to the selectivities (see Box), for the selections of the three libraries, Germ, Lim and Bnab against the two DNA targets (DNA1 and DNA2) and the two protein targets (prot1 and prot2). These results correspond to experiments where the 3 libraries are mixed in the initial population. The Lim library is outcompeted by the other two libraries when selected against the DNA1 target, which does not leave enough sequences to make a meaningful inference (see also Fig. S10 for more details on the sequence logos for the Bnab library). **C**. Sequence logos for $\tilde{s}_i(a)$ for the Germ and Lim libraries selected in isolation against the DNA1 target. For the Lim library, this palliates the absence of data in B. For the Germ library, it shows that essentially the same motifs are found whether the library is selected in a mixture as in B or on its own; the area under the logos is, however, different: it would be $\sigma^2/2$ with infinite sampling, but major deviations are caused by limited sampling (Fig. S9).

156 Remarkably, the Lim library behaves either like the Germ library or the BnAb library, depending on
 157 the target. In particular, a motif of positively charged amino acids emerges when selecting it against one of
 158 the two DNA targets (DNA1), but no clear motif emerges when selecting it against the other one (DNA2).
 159 Besides, when a clear motif emerges, it can be identical to the motif emerging from the Germ library as
 160 in case of a selection against the prot2 target, or different, as in the case of a selection against the DNA1
 161 target (but with a similar selection of positively charged amino acids).

162 3.2. Inter-library hierarchy

163 The hierarchy of selectivities between libraries is quantified by the parameter μ . This parameter also
 164 shows a pattern that is independent of the target: $\mu_{\text{Germ}, T} \simeq \mu_{\text{Lim}, T} < \mu_{\text{Bnab}, T}$ and even $\max_T(\mu_{\text{Germ}, T}, \mu_{\text{Lim}, T}) <$
 165 $\min_T(\mu_{\text{Bnab}, T})$ (Fig. 2B). Inferring μ is more challenging than inferring σ and the differences observed be-
 166 tween the Germ and Lim libraries are most likely not significant, as apparent from the observed variations
 167 between replicate experiments. The μ of the Bnab library is, on the other hand, systematically larger. The
 168 difference is explained by an experiment where selection is performed in the absence of DNA or protein tar-
 169 gets but in the presence of streptavidin-coated magnetic beads to which these targets are usually attached.

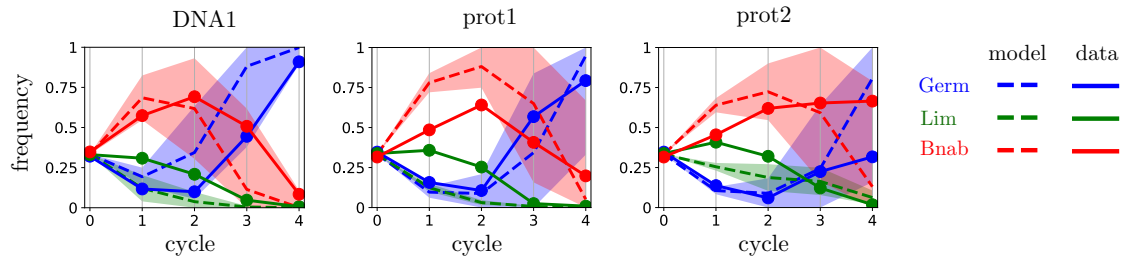


Figure 3: Dynamics of library frequencies – A mixture of the three libraries, Germ (blue), Lim (green) and Bnab (red) was subject to four successive cycles of selection and amplification against different targets. The full lines report the evolution of the relative frequencies of the three scaffolds. The dotted lines represent the estimated dynamics using the characterization of each library by a log-normal distribution with the parameters σ, μ estimated from the selection of the libraries against the same target (Appendix 1.4). The shaded area correspond to one standard deviation in the estimation of the parameters σ, μ . The model assumes that sequences are uniformly represented in each initial library, which is not the case in experiments and explains why the agreement with the data is only qualitative.

170 This experiment reproduces the differences in $\mu_{L,T}$, which indicates a small but significant affinity of the
 171 Bnab scaffold for the magnetic beads, independent of the sequence x (Fig. S12). While the differences in
 172 σ appear to be independent of the target, the differences in μ are thus related to a common feature of the
 173 targets. Given these different origins, the correlation between σ and μ that we observe may be fortuitous.

174 3.3. Implications for evolutionary dynamics

175 The different patterns of intra and inter-library hierarchies lead to a non-trivial evolutionary dynamics
 176 when selecting from an initial population that is composed of different libraries. In particular, a non-
 177 monotonic enrichment is expected when mixing two libraries characterized by (μ_1, σ_1) and (μ_2, σ_2) with
 178 $\mu_1 > \mu_2$ but $\sigma_1 < \sigma_2$: the library with largest μ dominates the first cycles while the one with largest σ
 179 dominates the later ones. This is indeed observed in experiments where different libraries are mixed in
 180 the initial population (Fig. 3). The dynamics of the relative frequencies of different libraries is globally
 181 predicted by a calculation of library frequencies in the mix based on the parameters (μ, σ) inferred for each
 182 library independently (Appendix 1.4), even though deviations are expected from the non-uniform sampling
 183 of sequences within each library, which is not encoded in σ or μ . Parametrizing the response to selection of
 184 a library by the two parameters (μ, σ) is thus not only useful to characterize its intrinsic response but also
 185 to rationalize the evolutionary dynamics of mixtures of libraries.

186 4. Discussion

187 How to interpret the result that intra-library diversity, as characterized by σ , decreases with the level of
 188 maturation of the scaffold? Here, we show that the parameter σ provides a characterization of intra-library
 189 diversity that is equivalent to three other approaches based on extreme value theory, information theory and
 190 sequence logs.

191 4.1. Extreme value statistics

192 In our previous work [14], we fitted the tail of the distribution of selectivities with generalized Pareto
 193 distributions, a family of distributions with two parameters, a shape parameter κ and a scaling parameter

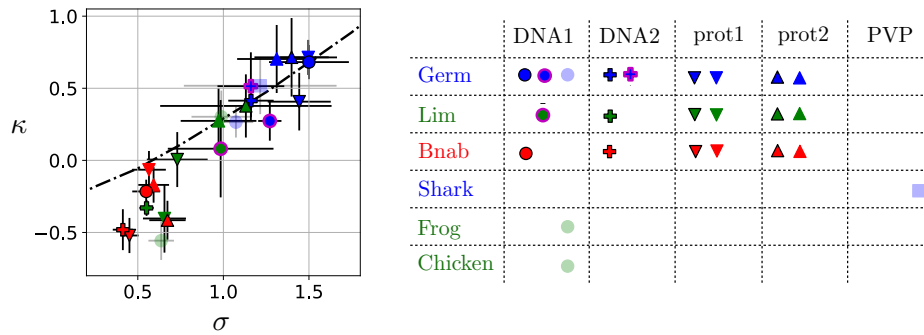


Figure 4: Shape parameter κ from fits of the selectivities to generalized Pareto distributions versus σ from fits to log-normal distributions – Results from different libraries selected against different targets are represented here with the same convention as in Figure 2: blue, green and red plain colors for the Germ, Lim and Bnab libraries, circle, cross, downward and upward triangles for the DNA1, DNA2, prot1 and prot2 targets. In addition, results from our previous work [14] are indicated in transparent blue if they involve a library built onto a germline scaffold and in transparent green if they involve a library built onto a matured scaffold. The hierarchy indicated by κ is essentially the same as the hierarchy indicated by σ , consistent with the expected relationship between κ and σ (black dotted line, Fig. S14). By the two approaches, libraries built onto germline scaffolds are found to have a more diverse response to selection than libraries built onto matured scaffolds irrespectively of the target (all values of σ and κ are given in Table 1).

194 τ . This was motivated by extreme value theory, which establishes that these parameters are sufficient to
 195 describe the tail of any distribution (Appendix 1.2). For different libraries L and different targets T , we
 196 found that generalized Pareto distributions provide a good fit of the upper tail of $P_{L,T}(s)$, with, depending
 197 on the scaffold L and target T either $\kappa > 0$ (heavy tail), $\kappa < 0$ (bounded tail) or $\kappa = 0$ (exponential tail).
 198 The origin of these different values of κ was, however, unclear.

199 Comparing probability-probability plots to assess the quality of the fits, our data appears equally well
 200 fitted by generalized Pareto distributions and log-normal distributions (Figs. S16-S22). This finding is at first
 201 sight puzzling as some of the fits with generalized Pareto distributions involve a non-zero shape parameter
 202 $\kappa \neq 0$ but extreme value theory states that the tail of log-normal distributions is asymptotically described
 203 by a shape parameter $\kappa = 0$ for all values of σ, μ [25]. Extreme value theory is, however, only valid in
 204 the double asymptotic limit $N \rightarrow \infty$ and $s^* \rightarrow \infty$, where N is the total number of samples and s^* the
 205 threshold above which these samples are considered. With finite data, determining whether this asymptotic
 206 regime is reached is notoriously difficult when the underlying distribution is log-normal [26]. More precisely,
 207 N points randomly sampled from a log-normal distribution with parameter σ are known to display an
 208 apparent $\kappa_N = \sigma / (2 \ln N)^{1/2}$ which tends to zero only very slowly with increasing values of N [26]. In fact,
 209 this relationship itself requires N (or σ) to be sufficiently large and finite size effects can even produce an
 210 apparent $\kappa_N < 0$ (Fig. S14).

211 While casting doubt on the practical applicability of extreme value theory, these statistical effects do not
 212 call into question the main conclusion of our previous work [14]: different combinations of scaffolds L and
 213 targets T exhibit different within-library hierarchies, which are quantified by the different values of their
 214 (apparent) shape parameter κ . Fits with a log-normal distribution provide another parameter σ that report
 215 essentially the same differences (Fig. 4). More importantly, we verify on our previous data, which partly
 216 involves different scaffolds and different targets, that libraries built on germline scaffolds have a higher σ
 217 than libraries built around matured scaffolds (Fig. 4 and Table 1).

218 4.2. Informational interpretation

219 The parameter σ can also be given an information-theoretic interpretation. From a statistical stand-
220 point, the specificity of selection of a population is naturally quantified by the relative entropy $D(f^1\|f^0) =$
221 $\sum_x f^1(x) \ln [f^1(x)/f^0(x)]$ which compares the distribution $f^1(x)$ of sequences x after one cycle of selection-
222 amplification to their initial distribution $f^0(x)$. When taking this initial distribution $f^0(x)$ to be a uniform
223 distribution over the N possible sequences, $f^0(x) = N^{-1}$, $f^1(x)$ is nothing but the selectivity $\tilde{s}(x)$ obtained
224 by choosing λ in Eq. (4) such that $\sum_x \tilde{s}(x) = 1$. The inverse of $D(\tilde{s}\|N^{-1})$ answers the following statis-
225 tical question (Appendix 1.3): how large should the initial population be to infer from the outcome of an
226 experiment that selection is at work? Assuming a large initial library with selectivity distribution $P(s)$,
227 $D(\tilde{s}\|N^{-1}) = \sum_x s(x) \ln [s(x)N]$ can be rewritten as

$$D(\tilde{s}\|N^{-1}) = \left\langle \frac{s}{\langle s \rangle} \ln \frac{s}{\langle s \rangle} \right\rangle \quad (2)$$

228 where the average is taken with $P(s)$, i.e., $\langle \phi(s) \rangle = \int_0^\infty ds P(s) \phi(s)$. When $P(s)$ is log-normal,

$$D(\tilde{s}\|N^{-1}) = \frac{\sigma^2}{2}, \quad (3)$$

229 showing that σ can be interpreted as quantifying the specificity of selection at the population level. This
230 statistical viewpoint can be extended to characterize the specificity of arbitrary sets of binders and lig-
231 ands (Appendix 1.3), generalizing a proposal to define specificity as an amount of information encoded in
232 interactions [27].

233 4.3. Sequence motifs

234 Assuming that the different sites i along the sequence contribute independently to the selectivity, $\tilde{s}(x) =$
235 $\prod_i \tilde{s}_i(x_i)$, the specificity $D(\tilde{s}\|N^{-1})$ is nothing but $\sum_i D(\tilde{s}_i\|A^{-1}) = \sum_i \sum_{a_i} \tilde{s}_i(a_i) \ln [\tilde{s}_i(a_i)A]$, the total area
236 under the sequence logos of $\tilde{s}_i(a)$, where $A = 20$ is the total number of amino acids. By displaying both
237 amino acid specificities and an overall measure of specificity of selection $D(\tilde{s}\|N^{-1})$, sequence logos thus
238 provide a convenient summary of selection within a library.

239 This comes, however, with an important caveat when selectivities are available only for a small subset
240 of $N' \ll N$ sequences, as it is the case in experiments. If ignoring unobserved sequences when computing
241 $\tilde{s}_i(a_i)$, the empirically determined quantity $\sum_i D(\tilde{s}_i\|A^{-1})$ overestimates the true value of $D(\tilde{s}\|N^{-1})$, all
242 the more as N' is smaller (Fig. S9). Because of this effect, the areas under the curve of the sequence
243 logos based on $\tilde{s}_i(a)$ are not comparable to $\sigma^2/2$ as Eq. (3) would suggest. They are also not comparable
244 across different experiments when the sampling sizes N' differ (Fig. 2B and C). Finally, even with $N' = N$,
245 deviations between $\sum_i D(\tilde{s}_i\|A^{-1})$ and $D(\tilde{s}\|N^{-1})$ may arise if the contributions of the different positions
246 are not additive.

247 5. Conclusion

248 In summary, we find that libraries built around germline antibody scaffolds have a response to selection
249 that is quantitatively different from libraries built around matured scaffolds: for arbitrary targets, they
250 contain sequences with a wider range of affinities, including specific sequences with the strongest affinities.

251 This constitutes the first quantitative evidence that germline antibodies are endowed with a special evo-
252 lutionary ability to generate selectable diversity. Our work was centered onto 3 libraries, one based on a
253 germline scaffold and two based on scaffolds derived from this germline scaffold with different degrees of
254 maturation, which we selected against 4 different targets. Assessing the generality of our conclusion will
255 require further experiments with additional scaffolds and targets. The statistical framework that we intro-
256 duced here provides the required tools to perform this analysis systematically and quantitatively. Beyond
257 the 3 libraries studied here, our conclusions are also supported by our previous results [14], which involved a
258 library built on another germline scaffold, 20 libraries built on other matured scaffolds, and a completely
259 different target (Fig. 4).

260 Which physical mechanisms may underly the differences in selective potential that we observe? A number
261 of studies, ranging from structural biology to molecular dynamics simulations, have reported changes in
262 antibody flexibility and target specificity over the course of affinity maturation [28, 29, 30, 31, 32, 33, 34, 35].
263 The emerging picture is that naïve antibodies are flexible and polyspecific and become more rigid and more
264 specific as they undergo affinity maturation. An increase of structural rigidity in the course of evolution
265 is also found in proteins unrelated to antibodies [36]. Germline scaffolds may thus be more flexible than
266 matured scaffolds. If this scenario is correct, how this structural flexibility translates into evolutionary
267 diversity once different complementary determining regions (CDRs) are grafted onto the scaffolds remains
268 to be explained.

269 Irrespectively of mechanisms, we described selectivity distributions of libraries with two statistical pa-
270 rameters, σ and μ , which we showed to be determined by different factors. Of these two parameters, σ , which
271 has simple physical and information-theoretic interpretations, is candidate to serve as a general quantitative
272 index of selective potential for biomolecules. Beyond selection, a next step is to extend this work to quantify
273 evolvability, i.e., the response to successive cycles of selection and mutations. Yet, being able to quantify
274 the selective potential of a scaffold by an index that is systematically reduced in the course of evolution
275 already raises an interesting challenge: can we increase this index to design libraries with better response
276 to selection?

277 Acknowledgments

278 This work was supported by FRM AJE20160635870 and by ANR-17-CE30-0021-02. It benefited from
279 the expertise of the high-throughput sequencing platform at the Institut de Biologie Intégrative de la Cellule
280 (I2BC) at Gif-sur-Yvette, France.

281 References

- 282 [1] G. P. Wagner, L. Altenberg, Perspective: complex adaptations and the evolution of evolvability, *Evolution* 50 (3) (1996)
283 967–976.
- 284 [2] M. Kirschner, J. Gerhart, Evolvability, *Proceedings of the National Academy of Sciences* 95 (15) (1998) 8420–8427.
- 285 [3] A. Wagner, *Robustness and evolvability in living systems*, Vol. 24, Princeton university press, 2013.
- 286 [4] L. Ancel Meyers, F. D. Ancel, M. Lachmann, Evolution of Genetic Potential, *PLoS computational biology* 1 (3) (2005)
287 e32.
- 288 [5] M. Parter, N. Kashtan, U. Alon, Facilitated Variation: How Evolution Learns from Past Environments To Generalize to
289 New Environments, *PLoS computational biology* 4 (11) (2008) e1000206.

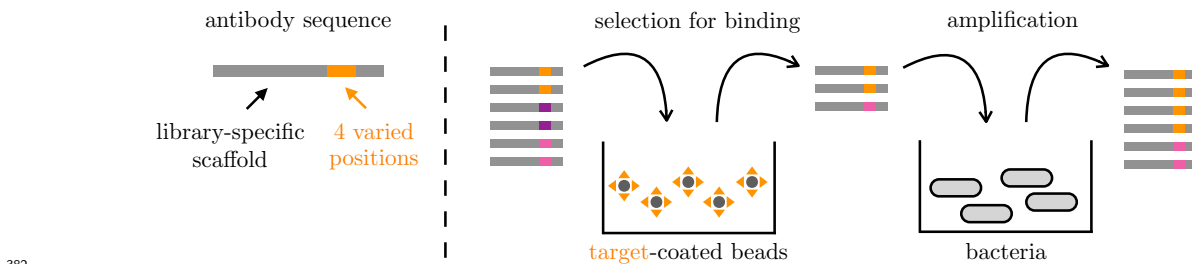
- 290 [6] M. Hemery, O. Rivoire, Evolution of sparsity and modularity in a model of protein allostery., *Physical review. E, Statistical,*
291 *nonlinear, and soft matter physics* 91 (4) (2015) 042704–10.
- 292 [7] A. Crombach, P. Hogeweg, Evolution of evolvability in gene regulatory networks, *PLoS computational biology* 4 (7) (2008)
293 e1000112.
- 294 [8] P. A. Romero, F. H. Arnold, Exploring protein fitness landscapes by directed evolution, *Nature reviews Molecular cell*
295 *biology* 10 (12) (2009) 866.
- 296 [9] J. D. Bloom, S. T. Labthavikul, C. R. Otey, F. H. Arnold, Protein stability promotes evolvability., *Proceedings of the*
297 *National Academy of Sciences* 103 (15) (2006) 5869–5874.
- 298 [10] E. Dellus-Gur, Á. Tóth-Petróczy, M. Elias, D. S. Tawfik, What makes a protein fold amenable to functional innovation?
299 Fold polarity and stability trade-offs., *Journal of Molecular Biology* 425 (14) (2013) 2609–2621.
- 300 [11] E. A. Padlan, Anatomy of the antibody molecule, *Molecular immunology* 31 (3) (1994) 169–217.
- 301 [12] H. R. Hoogenboom, Selecting and screening recombinant antibody libraries, *Nature Biotechnology* 23 (9) (2005) 1105–1116.
- 302 [13] H. N. Eisen, Affinity enhancement of antibodies: how low-affinity antibodies produced early in immune responses are
303 followed by high-affinity antibodies later and in memory B-cell responses, *Cancer immunology research* 2 (5) (2014)
304 381–392.
- 305 [14] S. Boyer, D. Biswas, A. Kumar Soshee, N. Scaramozzino, C. Nizak, O. Rivoire, Hierarchy and extremes in selections from
306 pools of randomized proteins., *Proceedings of the National Academy of Sciences of the United States of America* 113 (13)
307 (2016) 3482–3487.
- 308 [15] G. P. Smith, V. A. Petrenko, Phage Display, *Chemical Reviews* 97 (2) (1997) 391–410.
- 309 [16] D. M. Fowler, C. L. Araya, S. J. Fleishman, E. H. Kellogg, J. J. Stephany, D. Baker, S. Fields, High-resolution mapping
310 of protein sequence-function relationships, *Nature Methods* 7 (9) (2010) 741–746.
- 311 [17] D. R. Burton, P. Poignard, R. L. Stanfield, I. A. Wilson, Broadly neutralizing antibodies present new prospects to counter
312 highly antigenically diverse viruses., *Science* 337 (6091) (2012) 183–186.
- 313 [18] F. Klein, R. Diskin, J. F. Scheid, C. Gaebler, H. Mouquet, I. S. Georgiev, M. Pancera, T. Zhou, R.-B. Incesu, B. Z.
314 Fu, P. N. P. Gnanapragasam, T. Y. Oliveira, M. S. Seaman, P. D. Kwong, P. J. Bjorkman, M. C. Nussenzweig, Somatic
315 Mutations of the Immunoglobulin Framework Are Generally Required for Broad and Potent HIV-1 Neutralization, *Cell*
316 153 (1) (2013) 126–138.
- 317 [19] L. Pauling, D. Pressman, A. L. Grossberg, The serological properties of simple substances. vii. a quantitative theory of
318 the inhibition by haptens of the precipitation of heterogeneous antisera with antigens, and comparison with experimental
319 results for polyhaptenic simple substances and for azoproteins, *Journal of the American Chemical Society* 66 (5) (1944)
320 784–792.
- 321 [20] A. Nisonoff, D. Pressman, Heterogeneity and average combining constants of antibodies from individual rabbits., *Journal*
322 *of immunology (Baltimore, Md. : 1950)* 80 (6) (1958) 417–428.
- 323 [21] D. Lancet, E. Sadovsky, E. Seidemann, Probability model for molecular recognition in biological receptor repertoires:
324 significance to the olfactory system., *Proceedings of the National Academy of Sciences* 90 (8) (1993) 3715–3719.
- 325 [22] S. Rosenwald, R. Kafri, D. Lancet, Test of a statistical model for molecular recognition in biological repertoires., *Journal*
326 *of theoretical biology* 216 (3) (2002) 327–336.
- 327 [23] L. Wolf, O. K. Silander, E. van Nimwegen, Expression noise facilitates the evolution of gene regulation, *Elife* 4 (2015)
328 e05856.
- 329 [24] M. Smerlak, A. Youssef, Limiting fitness distributions in evolutionary dynamics., *Journal of theoretical biology* 416 (2017)
330 68–80.
- 331 [25] E. J. Gümbel, *Statistics of extremes*, Columbia Univ. Press, 1958.
- 332 [26] R. Perline, Strong, weak and false inverse power laws, *Statistical Science* 20 (1) (2005) 66–88.
- 333 [27] M. H. Huntley, A. Murugan, M. P. Brenner, Information capacity of specific interactions., *Proceedings of the National*
334 *Academy of Sciences of the United States of America* 113 (21) (2016) 5841–5846.
- 335 [28] G. J. Wedemayer, P. A. Patten, L. H. Wang, P. G. Schultz, R. C. Stevens, Structural insights into the evolution of an
336 antibody combining site, *Science* 276 (5319) (1997) 1665–1669.
- 337 [29] J. Yin, A. E. Beuscher IV, S. E. Andryski, R. C. Stevens, P. G. Schultz, Structural Plasticity and the Evolution of
338 Antibody Affinity and Specificity, *Journal of Molecular Biology* 330 (4) (2003) 651–656.
- 339 [30] J. R. Willis, B. S. Briney, S. L. DeLuca, J. E. Crowe, J. Meiler, Human germline antibody gene segments encode polyspecific
340 antibodies., *PLoS computational biology* 9 (4) (2013) e1003045.
- 341 [31] A. M. Sevy, T. M. Jacobs, J. E. Crowe, J. Meiler, Design of Protein Multi-specificity Using an Independent Sequence

- 342 Search Reduces the Barrier to Low Energy Sequences., *PLoS computational biology* 11 (7) (2015) e1004300.
- 343 [32] V. Manivel, N. C. Sahoo, D. M. Salunke, K. V. Rao, Maturation of an antibody response is governed by modulations in
344 flexibility of the antigen-combining site, *Immunity* 13 (5) (2000) 611–620.
- 345 [33] I. F. Thorpe, C. L. Brooks, Molecular evolution of affinity and flexibility in the immune system., *Proceedings of the*
346 *National Academy of Sciences* 104 (21) (2007) 8821–8826.
- 347 [34] T. Li, M. B. Tracka, S. Uddin, J. Casas-Finet, D. J. Jacobs, D. R. Livesay, Rigidity Emerges during Antibody Evolution in
348 Three Distinct Antibody Systems: Evidence from QSFR Analysis of Fab Fragments, *PLoS computational biology* 11 (7)
349 (2015) e1004327–23.
- 350 [35] M. C. Thielges, J. Zimmermann, W. Yu, M. Oda, F. E. Romesberg, Exploring the Energy Landscape of Antibody-Antigen
351 Complexes: Protein Dynamics, Flexibility, and Molecular Recognition, *Biochemistry* 47 (27) (2008) 7237–7247.
- 352 [36] E. C. Campbell, G. J. Correy, P. D. Mabbitt, A. M. Buckle, N. Tokuriki, C. J. Jackson, Laboratory evolution of protein
353 conformational dynamics., *Current Opinion in Structural Biology* 50 (2018) 49–57.
- 354 [37] T. D. Schneider, R. M. Stephens, Sequence logos: a new way to display consensus sequences, *Nucleic acids research* 18 (20)
355 (1990) 6097–6100.
- 356 [38] M. Djordjevic, A. M. Sengupta, Quantitative modeling and data analysis of selex experiments, *Physical biology* 3 (1)
357 (2005) 13.
- 358 [39] C. Rastogi, H. T. Rube, J. F. Kribelbauer, J. Crocker, R. E. Loker, G. D. Martini, O. Laptenko, W. A. Freed-Pastor,
359 C. Prives, D. L. Stern, R. S. Mann, H. J. Bussemaker, Accurate and sensitive quantification of protein-DNA binding
360 affinity., *Proceedings of the National Academy of Sciences of the United States of America* 115 (16) (2018) E3692–E3701.
- 361 [40] S. Coles, J. Bawa, L. Trenner, P. Dorazio, *An introduction to statistical modeling of extreme values*, Vol. 208, Springer,
362 2001.
- 363 [41] T. M. Cover, J. A. Thomas, *Elements of information theory*, John Wiley & Sons, 2012.

364 **BOX – Principles of antibody selection experiments**

365 We perform phage display experiments with different libraries of antibodies as input and different
 366 molecular targets (DNA hairpins or proteins) as selective pressures [15]. Our antibodies are single domains
 367 from the variable part of the heavy chain (V_H) of natural antibodies. Antibodies in a library share a
 368 common scaffold of $\simeq 100$ amino acids and differ only at four consecutive sites of their third complementary
 369 determining region (CDR3), which is known to be important for binding affinity and specificity. A library
 370 comprises all combinations of amino acids at these four sites and therefore consists of a total of $N = 20^4 \simeq 10^5$
 371 distinct sequences $x = (x_1, x_2, x_3, x_4)$. Initial populations include a total of 10^{11} sequences, corresponding
 372 to $\sim 10^6$ copies of each of the distinct $\sim 10^5$ sequences when a single library is considered. Physically, these
 373 populations are made of phages, each presenting at its surface one antibody and containing the corresponding
 374 sequence.

375 An experiment consists in a succession of cycles, each composed of two steps. In the first step, the
 376 phages are in solution with the targets, which are attached to magnetic beads and in excess relative to the
 377 phages to limit competitive binding (see Appendix 1.1). The beads are retrieved with a magnet and washed
 378 to retain the bound antibodies. In the second step, the selected phages are put in presence of bacteria which
 379 they infect to make new phages, thus amplifying retained sequences. A population of $\sim 10^{11}$ phages is thus
 380 reconstituted. Both the selection for binding to the target and the amplification can possibly depend on the
 381 sequence of the antibody.



383 We define the selectivity $s(x)$ of sequence x to be proportional to the probability for sequence x to
 384 pass one cycle. As the targets are in excess relative to the antibodies, selectivities are independent of the
 385 cycle c (see Appendix 1.1). In the limit of infinite population sizes, $s(x)$ is proportional to the relative
 386 enrichment $f^c(x)/f^{c-1}(x)$ of the frequencies $f^c(x)$ after any two successive cycles $c - 1$ and c . To estimate
 387 these selectivities, about 10^6 sequences are sampled before and after a cycle and read by high-throughput
 388 sequencing. Given the counts $n^{c-1}(x)$ and $n^c(x)$ of sequence x before and after cycle c , we estimate the
 389 selectivity of x as

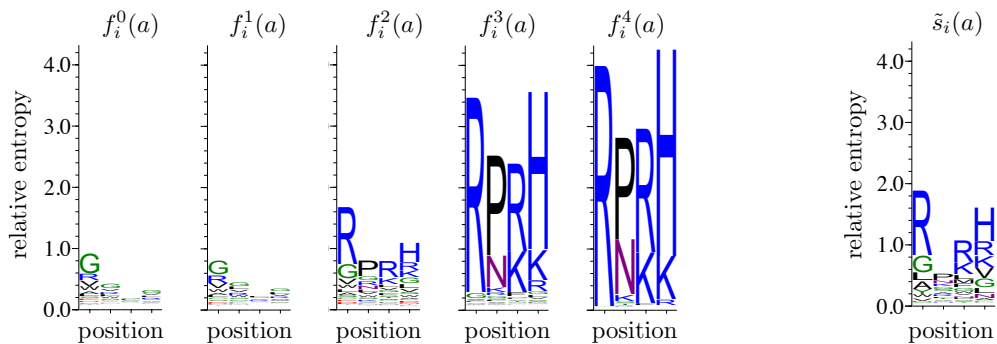
$$s(x) = \lambda \frac{n^c(x)}{n^{c-1}(x)} \quad (4)$$

390 where λ is an arbitrary multiplicative factor.

391 In practice, two types of noise must be taken into account when applying Eq. (4): an experimental
 392 noise, which implies that antibodies have a finite probability to pass a round of selection independently of
 393 their sequence, and a sampling noise, which arises from the limited number of sequence reads. This sampling
 394 noise is negligible if $n^{c-1}(x)$ and $n^c(x)$ are sufficiently large. This is generally not the case for any sequence

395 at the first cycle $c = 1$ where all $N = 20^4$ sequences are present in too small numbers but becomes the
 396 case at the third cycle $c = 3$ for the 100 to 1000 sequences with largest selectivities. We therefore compute
 397 $s(x)$ between the second and third cycles as $s(x) = \lambda n^3(x)/n^2(x)$ by restricting to sequences x that satisfy
 398 $n^2(x) \geq 10$ and $n^3(x) \geq 10$. Additionally, as the smallest selectivities are due to experimental noise, we
 399 retain only the sequences with $s(x) > s^*$ where s^* is determined self-consistently (Appendix 3.2 and Fig. S3).
 400 Selectivities $s(x)$ obtained by this procedure generally depend on the library (scaffold) L and the target T
 401 but are reproducible between independent experiments using the same library and the same target (Fig. S4).

402 To visualize the sequence dependence of selectivities, we use sequence logos [37]. In this representation,
 403 for each position i along the sequence, a bar of total height $\sum_a f_i^c(a) \ln [20 f_i^c(a)]$ is divided into letters, where
 404 each letter represents one of the 20 amino acids a with a size proportional to $f_i^c(a)$, the frequency of a at
 405 position i in the population after cycle c ; for instance, $f_2^c(a) = \sum_{x_1=1}^{20} \sum_{x_3=1}^{20} \sum_{x_4=1}^{20} f^c(x_1, a, x_3, x_4)$; finally,
 406 the letters are colored by chemical properties: polar in green, neutral in purple, basic in blue, acidic in
 407 red and hydrophobic in black. It illustrates how some motifs are progressively enriched over successions of
 408 selective cycles. This representation is, however, dependent on the frequencies $f^0(x)$ of sequences in the
 409 initial population. To eliminate this dependency, we define an effective frequency $\tilde{s}_i(a)$ per position i and
 410 amino acid a as $\tilde{s}_i(a) = \sum_x s(x) \delta(x_i, a) / \sum_x s(x)$, which would correspond to the frequency of a at position
 411 i after one round of selection if all sequences x were uniformly distributed in the initial population. It can
 412 also be represented by a sequence logo but depends only on $s(x)$, as illustrated here by the Germ library
 413 selected against the DNA1 target (see Figs. S5-S7 for other cases):



414

SUPPLEMENTARY INFORMATION

415

416 1. Theoretical methods

417 1.1. Physics of selection

418 1.1.1. Selectivities and binding energies

419 When assuming that selection is controlled by equilibrium binding to the target, the distribution of
 420 selectivities is constrained by physical principles. Starting with a population of identical antibodies A and a
 421 single target T in excess relative to antibodies, $[T]_{\text{tot}} \gg [A]_{\text{tot}}$, the probability for an antibody to be bound
 422 to a target is

$$s_{AT} = \frac{[AT]_{\text{eq}}}{[AT]_{\text{eq}} + [A]_{\text{eq}}} = \frac{1}{1 + K_{AT}[T]_{\text{eq}}^{-1}} \simeq \frac{1}{1 + K_{AT}[T]_{\text{tot}}^{-1}} \quad (5)$$

423 where $[AT]_{\text{eq}}$ and $[A]_{\text{eq}}$ are, respectively, the equilibrium concentration of bound and free antibodies and
 424 where $K_{AT} = [A]_{\text{eq}}[T]_{\text{eq}}/[AT]_{\text{eq}}$ is the dissociation constant that characterizes the equilibrium. We used
 425 here the fact that most of the targets are unbound so that $[T]_{\text{eq}} = [T]_{\text{tot}} - [AT]_{\text{eq}} \simeq [T]_{\text{tot}}$, which is
 426 justified for our experiments where the total number of targets far exceeds the total number of antibodies,
 427 $[AT]_{\text{eq}} < [A]_{\text{tot}} \ll [T]_{\text{tot}}$. The dissociation constant can also be written as $K_{AT} = k_-/k_+$, where k_+ and k_-
 428 denote respectively the association and dissociation rates of an antibody-target pair.

429 We can equivalently write

$$s_{AT} = \frac{1}{1 + e^{\beta(\Delta G_{AT} - \mu)}} \quad (6)$$

430 by introducing a binding free energy $\Delta G_{AT} = \beta^{-1} \ln K_{AT}$ and a chemical potential $\mu = \beta^{-1} \ln [T]_{\text{tot}}$, where
 431 β sets the energy scale [38]. This Fermi-Dirac statistics is approximated by a Boltzmann statistics

$$s_{AT} \simeq e^{-\beta(\Delta G_{AT} - \mu)}. \quad (7)$$

432 when $\Delta G_{AT} \gg \mu$. This approximation is justified when $[T]_{\text{tot}} \ll K_{AT}$ or, equivalently, $[AT]_{\text{eq}} \ll [A]_{\text{eq}}$, i.e.,
 433 when the concentration of the targets or the binding affinity are sufficiently low for most of the antibodies
 434 to be unbound. Working in this regime is important for the selectivities to reflect binding free energies.
 435 Otherwise, the targets are saturating, which cause antibodies to be bound with high probability irrespectively
 436 of their dissociation constant.

437 These conclusions are unchanged when considering a population consisting of different antibodies A with
 438 different dissociation constants K_{AT} and binding free energies $\Delta G_{AT} = \beta^{-1} \ln K_{AT}$. In summary, when
 439 considering different antibodies A , each with its own dissociation constant K_{AT} , the choice of the target
 440 concentration $[T]_{\text{tot}}$ is subject to the two constraints

$$\sum_A [A]_{\text{tot}} \ll [T]_{\text{tot}} \ll \min_A K_{AT}. \quad (8)$$

441 The first constraint $\sum_A [A]_{\text{tot}} \ll [T]_{\text{tot}}$ guarantees an absence of competition between antibodies so that
 442 the selectivities s_{AT} are intrinsic properties of the sequences of A , independent of the composition of the
 443 population and therefore independent of the round c when successive cycles of selection are performed;
 444 formally, $[T]_{\text{eq}}$, which depends on all A present, can then be replaced by $[T]_{\text{tot}}$ in Eq. (5). The second

445 constraint $[T]_{\text{tot}} \ll \min_A K_{AT}$ guarantees that even the best binders are not in a saturation regime with
 446 $s_A \simeq 1$ independently of differences in their dissociation constants K_{AT} . In our phage display experiments,
 447 $\sum_A [A]_{\text{tot}} \simeq 10^{11} \text{ mL}^{-1}$ and $[T]_{\text{tot}} \simeq 10^{14} \text{ mL}^{-1}$, which satisfies the first constraint. The concentration
 448 $\sum_A [AT]_{\text{eq}}$ of selected antibodies before amplification is estimated between 10^5 mL^{-1} at the first round
 449 of selection and $10^7 - 10^8 \text{ mL}^{-1}$ at the fourth. Considering this last number to reflect properties of the
 450 best binders, we estimate that $\min_A K_{AT}/[T]_{\text{tot}} \simeq \sum_A [AT]_{\text{eq}}/\sum_A [A]_{\text{tot}} \simeq 10^3$, which satisfies the second
 451 constraint.

452 1.1.2. Justification and limitations of log-normal distributions

453 Assuming an additive model for the interaction where the binding energy between sequence $x = (x_1, \dots, x_\ell)$
 454 and its target takes is of the form $\Delta G(x) = \sum_{i=1}^{\ell} \epsilon_i(x_i)$ with the $\epsilon_i(x_i)$ taking random values, the central
 455 limit theorem indicates that for sufficiently large ℓ the energies $\Delta G(x)$ are distributed normally with a mean
 456 $\mu \simeq -\ell \langle \epsilon \rangle$ and a variance $\sigma^2 \simeq \ell (\langle \epsilon^2 \rangle - \langle \epsilon \rangle^2)$, where $\langle \epsilon \rangle$ and $\langle \epsilon^2 \rangle - \langle \epsilon \rangle^2$ are respectively the mean and variance
 457 of the values of binding energies per position $\epsilon_i(x_i)$. Given Eq. (7), this leads to a log-normal distribution
 458 for the selectivities $s(x) \propto e^{-\beta \Delta G(x)}$.

459 The assumptions involved in this derivation may not be justified, starting from the assumption that
 460 selectivity can be equated to binding affinity. However, essentially all deviations from this model, sequence-
 461 dependent amplification differences, saturation of the targets, multiple binding sites or non-additive interac-
 462 tions, can be incorporated in a more refined model, at the expense of introducing additional parameters [39].
 463 Deviations from a log-normal distribution of selectivities can therefore, at least in principle, be systematically
 464 analyzed and understood.

465 1.2. Statistics of selection

466 1.2.1. Extreme value statistics

467 Extreme value theory states that for any probability distribution $\mathbb{P}(S)$, the probability to have $S = s \geq s^*$
 468 conditioned to $S \geq s^*$ converges to a generalized Pareto distribution $f_{\kappa, s^*, \tau}(s) = \tau^{-1} f_{\kappa}((s - s^*)/\tau)$ as
 469 $s^* \rightarrow \infty$ [40], where

$$f_{\kappa}(x) = \begin{cases} (1 + \kappa x)^{-(1 + \frac{1}{\kappa})} & \text{if } \kappa \neq 0, \\ e^{-x} & \text{if } \kappa = 0. \end{cases} \quad (9)$$

470 The shape parameter κ is determined by the tail of the distribution of S . In particular, $\kappa < 0$ for bounded
 471 distributions and $\kappa = 0$ for distributions with exponentially decreasing tails, including log-normal distribu-
 472 tions. On the other hand, $\kappa > 0$ for distributions whose tail decays as a power-law. For such distributions,
 473 when considering a large number N of random values $s_1 > s_2 > \dots > s_N$, $s_r \sim s_1 r^{-\kappa}$ for $r \ll N$, which
 474 is represented in a log-log plot of s_r versus the rank r by the linear relationship $\ln(s_r/s_1) \sim -\kappa \ln r$ for the
 475 smallest values of r .

476 1.2.2. Effective shape parameter of log-normal distributions

477 In the asymptotic limit where $N \rightarrow \infty$ followed by $s^* \rightarrow \infty$, log-normal distributions are described by a
 478 shape parameter $\kappa = 0$, but their tail decays only slowly. As a result, a large but finite number N of random
 479 values drawn from a log-normal distribution may appear to be drawn from a distribution with a non-zero
 480 shape parameter $\kappa_N \neq 0$.

481 More precisely, it can be shown that N values $s_1 > s_2 > \dots > s_N$ drawn from a log-normal distribution
 482 with parameters σ, μ satisfy for $r \ll N$ the relation

$$\mathbb{E}[\ln s_r] \simeq \mu + \sigma(2 \ln N)^{1/2} - \sigma(2 \ln N)^{-1/2} \ln r, \quad (10)$$

483 which corresponds to an apparent shape parameter $\kappa_N = \sigma(2 \ln N)^{-1/2}$ [26]. As κ_N vanishes only very
 484 slowly with N , it is difficult to determine whether N data points arise from a log-normal distribution or
 485 from a distribution with a shape parameter $\kappa > 0$. For instance, increasing the sample size from $N = 10^5$
 486 to $N = 10^6$ changes κ_N by only 8%.

487 Eq. (10) itself assumes that N is large enough. Numerically, we observe that for a given value of N , it
 488 breaks down when σ is below some value σ^* . In such cases, the data may appear to arise from a bounded
 489 distribution with $\kappa_N < 0$. Fig. S14 shows the relationship between κ_N and σ obtained from numerical
 490 simulations when fixing $N = 10^4$ and $\mu = 0$, in which case $\sigma^* \simeq 0.5$. The same relationship appears as a
 491 black dotted line in Fig. 4.

492 1.3. Information theory of selection

493 1.3.1. Relative entropies

494 A general statistical approach to quantify how random variables drawn from a probability P^1 are con-
 495 sistent with a reference probability distribution P^0 is to use their relative entropy $D(P^1 \| P^0)$, also known
 496 as the Kullback-Leibler divergence [41], which is defined by

$$D(P^1 \| P^0) = \sum_x P^1(x) \ln \frac{P^1(x)}{P^0(x)}. \quad (11)$$

497 The inverse of this quantity corresponds roughly to the number of samples required to discriminate P^1 from
 498 P^0 . More precisely, the probability under P^0 of N samples drawn from P^1 scales as $e^{-ND(P^1 \| P^0)}$ [41].

499 1.3.2. Information theory of specific interactions

500 The problem of quantifying specificity arises when two classes of objects or properties A and T may
 501 be associated. If this association is described by the probability $P^1(A, T)$ that A is associated with T ,
 502 a natural measure of specificity is $D(P^1 \| P^0)$ where $P^0(A, T)$ represents the expectation from random as-
 503 sociations. If $P^0(A, T) = P^1(A)P^1(T)$ where $P^1(A) = \sum_T P^1(A, T)$ and $P^1(T) = \sum_A P^1(A, T)$ are the
 504 marginal distributions of A and T , $D(P^1 \| P^0)$ corresponds to the mutual information $I(A; T)$ between the
 505 random variables A and T [41]. This choice of P^0 , however, generally does not reflect the expectation from
 506 random associations and the relevant measure of specificity is therefore generically not captured by a mutual
 507 information but by the more general relative entropy $D(P^1 \| P^0)$.

508 In the case of association between a set of ligands A and a set of targets T controlled by equilibrium
 509 binding, the probability $P^1(A, T)$ to find A bound to T is

$$P^1(A, T) = \frac{[AT]_{\text{eq}}}{[A]_{\text{eq}} + \sum_{T'} [AT']_{\text{eq}}} \simeq \frac{[AT]_{\text{eq}}}{[A]_{\text{eq}}} = K_{AT}^{-1} [T]_{\text{eq}} \simeq K_{AT}^{-1} [T]_{\text{tot}} \quad (12)$$

510 where K_{AT} is the dissociation constant between A and T and where the approximations are justified in

511 Appendix 1.1. A random association is defined here by considering equal dissociation constants,

$$P^0(A, T) = \frac{[A]_{\text{tot}}[T]_{\text{tot}}}{\sum_{A', T'} [A']_{\text{tot}}[T']_{\text{tot}}}. \quad (13)$$

512 This distribution generally differs from $P^1(A)P^1(T)$.

513 A selectivity s_{AT} can be defined for each pair A, T as $s_{AT} = P^1(A, T)/P^0(A, T)$ so that

$$D(P^1 \| P^0) = \left\langle \ln \left(\frac{P^1}{P^0} \right) \right\rangle_1 = \sum_{A, T} P^1(A, T) \ln \frac{P^1(A, T)}{P^0(A, T)} = \sum_{A, T} P^0(A, T) s_{AT} \ln s_{AT} = \langle s \ln s \rangle_0 \quad (14)$$

514 where $\langle \cdot \rangle_0$ and $\langle \cdot \rangle_1$ denote averages taken with $P^0(A, T)$ and $P^1(A, T)$ respectively.

515 More generally, $s_{AT} = \lambda P^1(A, T)/P^0(A, T)$ with an arbitrary multiplicative constant λ that can always
516 be written $\lambda = \langle s \rangle_0$. This corresponds to replacing s by $s/\langle s \rangle_0$ in the previous formula,

$$D(P^1 \| P^0) = \left\langle \frac{s}{\langle s \rangle_0} \ln \frac{s}{\langle s \rangle_0} \right\rangle_0 \quad (15)$$

517 This is equivalent to Eq. (2) where a single target T is considered and where $P^0(A, T) = 1/N$ and $P^1(A, T) =$
518 $s(x)$ with x representing the sequence of A . This relationship is valid for any initial distribution $f^0(x)$ as
519 long as $f^1(x) \propto s(x)f^0(x)$.

520 The identity

$$D(s \| N^{-1}) = \left\langle \frac{s}{\langle s \rangle} \ln \frac{s}{\langle s \rangle} \right\rangle \quad (16)$$

521 where averages $\langle \cdot \rangle$ are now taken with a distribution $P(s)$ of the selectivities over the different sequences
522 x is, however, valid only when considering as initial distribution a uniform distribution over the sequences.
523 The notation $D(s \| N^{-1})$ assumes, besides, that $\sum_x s(x) = 1$ so that $s(x)$ can be interpreted as a probability
524 distribution.

525 1.3.3. Equivalence with the parameter σ

526 If further assuming that $P(s)$ is a log-normal distribution with parameters σ and μ , $\langle s \rangle = e^{\mu + \sigma^2/2}$ and
527 $\langle s \ln s \rangle = \langle s \rangle(\mu + \sigma^2)$ so that

$$D(s \| N^{-1}) = \frac{\sigma^2}{2} \quad (17)$$

528 irrespectively of the value of μ . This reflects the fact that specificity quantifies only relative differences in
529 binding free energies between different ligands.

530 A previous study proposed the mutual information as a measure of specificity [27]. It is justified, however,
531 only within the special model considered in [27] where, because of the overall symmetry of the interactions
532 between the M locks A and M keys T , $P^1(A) \simeq P^1(T) \simeq 1/M$, and therefore $P^0(A, T) = 1/M^2 \simeq$
533 $P^1(A)P^1(T)$.

534 *1.4. Dynamics of selection*

535 *1.4.1. Recursion for the sequence frequencies*

536 If $N^c(x)$ denotes the number of copies of sequence x at cycle c , the dynamics of selection satisfies the
537 recursion

$$N^c(x) = \alpha_c s(x) N^{c-1}(x) \quad (18)$$

538 where α_c represents an amplification factor to reach at every round the same total population size N , i.e.,
539 $\sum_x N^c(x) = N$ independent of c . In terms of frequencies $f^c(x) = N^c(x)/N$, this gives $\alpha_c = (\sum_x s(x) f^c(x))^{-1}$
540 and

$$f^c(x) = \frac{s(x) f^{c-1}(x)}{\sum_{x'} s(x') f^{c-1}(x')} = \frac{(s(x))^c f^0(x)}{\sum_{x'} (s(x'))^c f^0(x')}. \quad (19)$$

541 These recursions assume a large N , so that the frequencies $f^c(x) = N^c(x)/N$ are meaningful; in particular,
542 they assume that no sequence disappears.

543 Note the similarity with a Boltzmann distribution with the cycle c playing the role of an inverse tem-
544 perature.

545 *1.4.2. Recursion for the library frequencies*

546 When considering a population consisting of an equal mix of different libraries L , the frequency $f^c(L) =$
547 $\sum_{x \in L} f^c(x)$ of library L satisfies the recursion

$$f^c(L) = \frac{\langle s^c \rangle_L}{\sum_{L'} \langle s^c \rangle_{L'}} \quad (20)$$

548 with

$$\langle s^c \rangle_L = \sum_{x \in L} (s(x))^c f^0(x) = \int_0^\infty ds P_L(s) s^c = \exp\left(c\mu_L + \frac{c^2\sigma_L^2}{2}\right). \quad (21)$$

549 Here, the first equality defines the average $\langle \cdot \rangle_L$ within each library L . The second equality, on the other
550 hand, makes two assumptions: first, that selectivities s within library L are described by a distribution
551 of selectivities $P_S(s)$ and, second, that sequences within a library are uniformly represented in the initial
552 population. The third equality makes the additional assumption that $P_L(s)$ is a log-normal distribution
553 with parameters σ_L and μ_L .

554 Under these different assumptions, the frequency of library L at cycle c is given by

$$f^c(L) = \left(\sum_{L'} e^{c(\mu_{L'} - \mu_L) + c^2(\sigma_{L'}^2 - \sigma_L^2)/2} \right)^{-1}. \quad (22)$$

555 This shows that for small c , the dynamics is controlled by the μ_L , with in limit $c \rightarrow 0$, $(f^c(L) - f^0(L))/f^0(L) \simeq$
556 $c(\mu_L - \langle \mu \rangle)$, i.e., at the first cycle, the frequency of library L increases if its μ_S exceeds the average $\langle \mu \rangle$
557 across libraries and it decreases otherwise. For large c , on the other hand, the dynamics is controlled by the
558 σ_L s with $f^c(L) \rightarrow 1$ for the library L that has largest σ_L , regardless of the values of μ_L .

559 These calculations rely on several assumption, in particular the assumption that sequences within a
560 library have initially uniform frequencies, which is not satisfied in the experiments. This explains the
561 differences between the model and the data in Fig. 3.

562 2. Experimental methods

563 Experimental methods are as in our previous work [14], except for target immobilization and sequencing
564 data analysis as summarized below.

565 2.1. Phage production

566 Production of antibody-displaying phage was performed through infection of library cells (TG1 strain)
567 with M13KO7 helper phage and growth at 30°C for 7 h in selective 2xYT medium containing 100 µg/mL
568 ampicillin (Sigma-Aldrich, Saint-Louis, MO, USA). Cells were then centrifuged and the supernatant con-
569 taining displaying phages was kept and stored at 4°C overnight. All selections were performed on the day
570 immediately following the phage production step.

571 2.2. Target immobilization

572 Target molecules were immobilized on streptavidin-coated magnetic beads (Dynabeads(R) M-280 Strep-
573 tavidin) purchased from Invitrogen Life Technologies (Carlsbad, CA, USA). The DNA hairpin targets (DNA1
574 and DNA2) in fusion with a biotin at their 5' end were purchased from IDT (Leuven, Belgium) diluted in
575 MilliQ water and stored at -20°C. The genes of protein targets (eGFP and mCherry, corresponding re-
576 spectively to PDB IDs 2Y0G and 2H5Q) in fusion with a SBP tag were kindly provided by Sandrine Moutel
577 (Institut Curie, Paris, France). They were produced in liquid T7 Express *E. Coli* cultures induced at
578 OD₆₀₀ = 0.5 with 300 µM Isopropyl β-D-1-thiogalactopyranoside (IPTG, Sigma-Aldrich, Saint-Louis, MO,
579 USA) final and incubated overnight at 30°C. The proteins were harvested by threefold flash freezing in
580 liquid nitrogen and quick thawing in a water bath at 42°C, followed by incubation with 50 µg/mL lysozyme
581 final and 2.5 U/mL DNase I final at 30°C for 15 minutes and centrifugation at 15,000 g and 4°C for 30
582 minutes. The supernatant was aliquoted in protein low-bind tubes (Protein LoBind, Eppendorf, Hamburg,
583 Germany), flash frozen in liquid nitrogen and stored at -80°C until use.

584 Binding of target molecules to streptavidin-coated magnetic beads was performed in DNA low-bind
585 tubes (DNA LoBind tubes, Eppendorf, Hamburg, Germany) for the DNA targets or protein low-bind tubes
586 (Protein LoBind tubes, Eppendorf, Hamburg, Germany) for the protein targets. Beads and targets were
587 incubated in 0.5x PBS at ambient temperature on a rocker for 15 min, followed by removal of all liquid
588 and 3 washing steps: addition of 500 µL washing solution, vortexing, separation of beads using a magnet
589 and removal of all liquid. Finally, the beads were stored in washing buffer at 4°C for use on the following
590 day. Bw1X buffer (1 M NaCl, 5 mM Trizma at pH = 7.4, 0.5 mM EDTA) was used as washing buffer for
591 DNA targets (to screen electrostatic interactions), 1x PBS with 0.1 % Tween20 for protein targets (to screen
592 hydrophobic interactions). The same procedure was followed for negative/null selection tubes, with MilliQ
593 water instead of target solutions.

594 Successful immobilization of protein targets was confirmed by fluorescence measurements of treated beads
595 against untreated and MilliQ water-treated beads as negative controls.

596 2.3. Phage display selection

597 The selection protocol is as previously published in [14]. The washing buffer was removed from the
598 target-covered beads. Then, 1 mL of culture supernatant from the phage production step containing $\approx 10^{11}$
599 phages was added to the negative selection tube (containing no targets) and incubated for 90 minutes at

600 ambient temperature, shaking. The beads were separated by a magnet and the liquid was transferred to the
601 positive selection tube (containing the targets) and incubated for 90 minutes at room temperature, shaking.
602 Finally, all liquid containing unbound phage was removed and the beads were subjected to a 10-fold washing
603 using 10 mL of 1x PBS with 0.1% Tween20. Bound phage were eluted from beads with 1.4% triethylamine
604 (Sigma-Aldrich, Saint-Louis, MO, USA) in MilliQ water and used for infection of fresh exponential TG1
605 cells to obtain the selected library.

606 *2.4. Illumina sequencing*

607 Glycerol stocks of library cells at relevant selection cycles were defrosted and plasmids were extracted
608 using purification kits from Macherey-Nagel (Düren, Germany). No liquid culture was performed prior to
609 plasmid extraction to avoid potential additional biases from growing an overnight culture beforehand. Re-
610 sulting plasmids were used as input for Illumina sequencing preparation PCR: a first reaction using primer
611 sequences common to all three libraries downstream CDR₃ (GCTCGAGACGGTAACCAGG, forward) and halfway
612 inside V_H (ACAACCCGTCTCTTAAGTCTCGT, reverse) added random barcodes of length 5 nt to discriminate be-
613 tween neighboring clusters. A second reaction added P5 and P7 indices to identify library, target and
614 selection round corresponding to each cluster, as well as the adapter for the sequencing procedure. Illumina
615 sequencing and demultiplexing were performed at I2BC, Gif-sur-Yvette, France.

616 **3. Data analysis**

617 *3.1. Preprocessing*

618 The Illumina sequencing yields for each sample (i.e., each library, target and selection round) between 10⁵
619 and 5.10⁶ sequencing clusters. The data files contain the entirely overlapping forward and reverse reads for
620 all clusters of a given sample. Each cluster was accepted or discarded based on the following procedure: Both
621 the forward and reverse reads were screened for the presence of the primer sequences (up to 4 nt mismatch
622 accepted for each) and cut to keep only the part between the primers (including the primers). Either one
623 was discarded if the primer search was unsuccessful. We then checked if the remaining forward and/or
624 reverse sequence fragments have the expected length of 170 nt, corresponding to the region of interest. If
625 only one direction had the expected length, only this direction was kept and the other one was discarded. If
626 both directions did not have expected length, the complete cluster was discarded. Finally, if both reads had
627 expected length, a consensus sequence was generated by taking on each position with disagreement between
628 both reads the nucleotide measured with highest quality read. A final check was performed for (i) a sufficient
629 average quality read over the whole region of interest ($\langle Q \rangle \geq 59$) and (ii) the restriction sites immediately
630 up- and downstream CDR₃ (TGTGCGCGC and TTCGACTAC) are located at their expected positions (108-116
631 and 129-137 in reverse direction; up to 4 nt mismatch accepted for each). The cluster was discarded if either
632 of these two criteria was not fulfilled.

633 After completion of this procedure, (i) the framework (Germ, Lim or Bnab) and (ii) the CDR3 sequence
634 for all remaining sequencing reads in the full-library experiments were identified. Step (i) was performed
635 by measuring the Hamming distance of the visible library-specific framework part upstream the CDR3 of
636 the read (of length 116 nt) to all three framework reference sequences. The read was assigned to the nearest
637 framework if the Hamming distance to the nearest framework was ≤ 7 nt *and* the difference in Hamming
638 distance to the nearest and next-nearest frameworks was ≥ 3 nt. For step (ii), the CDR3 sequence was

639 simply extracted from the read for the full-library experiments. For the selections with reduced diversity a
 640 similar procedure as for the framework part was applied: the measured CDR3 sequence was assigned to the
 641 nearest among ~ 20 reference sequences if the Hamming distance was ≤ 3 nt and the difference in Hamming
 642 distance between nearest and next-nearest was ≥ 1 nt. After assessment of the sequence identity of all
 643 clusters in a dataset, the CDR3 sequences were translated into amino acids and the number of occurrences
 644 of each clone (determined by its framework and its CDR3 sequence) was counted.

645 The nucleotide sequences of the visible framework parts upstream the CDR3 of all three libraries as well
 646 as the Hamming distances d_H between the pairs is as follows:

647 Germ:

648 ACAACCCGTCTCTTAAGTCTCGTGTTACCATCTCTGTTGACACCTCTAAAAACCAGTT . . .
 649 CTCTCTGAAACTGTCTTCTGTTACTGCGGCGGACACTGCGGTTTACTACTGTGCGCGC

650 Lim:

651 ACAACCCGTCTCTTAAGTCTCGTGTTACCATCTCTATCGACACCTCTAAAAACCACTT . . .
 652 CTCTCTGCGTCTGATCTCTGTTACTGCGGCGGACACTGCGGTTTACCACTGTGCGCGC

653 Bnab:

654 ACAACCCGTCTCTTAAGTCTCGTCTGACCCTGGCGCTGGACACCCGAAAAACCTGGT . . .
 655 TTTCTGAAACTGAACTCTGTTACTGCGGCGGACACCGCGACCTACTACTGTGCGCGC

656 $d_H(\text{Germ}, \text{Lim}) = 10$ nt, $d_H(\text{Lim}, \text{Bnab}) = 25$ nt and $d_H(\text{Germ}, \text{Bnab}) = 22$ nt.

657 For the mixed full-library selections, final data files contain three columns: 1) framework identity ('germ'
 658 for Germline, 'lmtd' for Limited, 'bnAb' for Bnab, '????' if framework inference failed), 2) CDR3 identity
 659 given by the sequence of 4 amino acids or the sequence of 12 nucleotides or by '????' if the CDR3 readout
 660 failed, 3) number of occurrences in the dataset. The preprocessed data from the experiments reported in
 661 this paper is made available in this format.

662 We checked that the results are unaffected by the choice of the parameters in the preprocessing procedure
 663 described here.

664 3.2. Noise cleaning

665 Selectivities are computed from sequencing counts as indicated in Eq. 4. To account for sampling noise,
 666 only sequences whose count is ≥ 10 both at round c and $c+1$ are considered. Moreover, we ignore selectivities
 667 $s(x)$ below a threshold s^* , which arise from unspecific binding. Unspecific binding modifies the expression
 668 for the selectivity of sequence x to include a sequence-independent unspecific binding energy ΔG_{us} ,

$$s(x) = \frac{e^{-\beta\Delta G(x)} + e^{-\beta\Delta G_{\text{us}}}}{1 + e^{-\beta\Delta G(x)} + e^{-\beta\Delta G_{\text{us}}}}. \quad (23)$$

669 It sets a lower bound for the selectivity given by

$$s_{\text{us}} = \frac{e^{-\beta\Delta G_{\text{us}}}}{1 + e^{-\beta\Delta G_{\text{us}}}} = \frac{1}{1 + e^{\beta\Delta G_{\text{us}}}}. \quad (24)$$

670 The argument for log-normality of selectivity distributions applies only when the specific binding contribution
 671 $\Delta G(x)$ dominates the selectivity. We therefore eliminate the selectivities dominated by unspecific binding.

672 This is done by introducing a cut-off s^* . The choice is made such that (i) the values of the inferred
 673 parameters $\hat{\sigma}$ and $\hat{\mu}$ are approximately constant for all $s \geq s^*$ and (ii) s^* is large enough to eliminate

674 selectivities due to unspecific binding. This last condition is implemented by plotting the counts $n^2(x)$ and
 675 $n^3(x)$ at the two successive cycles, as illustrated in Figure S3: sequences with $s = s_{\text{us}}$ appear in the diagonal
 676 with a variance that decreases with increasing counts, as expected from sampling noise, and s^* is chosen so
 677 as to exclude these sequences. In cases where specific binding to the target is very strong, sequences selected
 678 for unspecific binding are not present (Fig. S15A), while in cases where specific binding is too weak, only
 679 sequences selected for unspecific binding are present (Fig. S15F).

680 The same criteria apply when fitting to generalized Pareto distributions to infer the parameter κ but
 681 criterion (i) may lead to a higher value of s^* if the measured selectivities extend beyond the tail of the
 682 distribution. In our previous work [14], we only considered criterion (i). In one case (Frog3 against DNA1),
 683 the s^* that we define here by accounting for (ii) differs from the s^* that had previously defined (Fig. S15),
 684 which leads to a significantly different estimation of κ : $\hat{\kappa} = -0.53 \pm 0.19$ instead of $\hat{\kappa} = 0.97 \pm 0.38$. In the
 685 other cases, we recover essentially the same results. The new analysis provides, however, additional insights;
 686 in the case of Frog3 against PVP, it thus appear that the vanishing value of κ can be attributed to the
 687 selectivities being dominated by unspecific binding (Fig. S15).

688 3.3. Fit to log-normal distributions

689 To infer from experimental data the parameters σ and μ of a log-normal distribution, as given by Eq. (1),
 690 we focus on the best available selectivities $s_i > s^*$, the log-normal distribution is under-sampled. In practice,
 691 it is more convenient to work with the log of the selectivities, $y_i = \ln s_i$, and to fit them with a normal
 692 distribution. If restricting to values y_i larger than a given threshold y^* , the probability $\mathbb{P}[Y = y|Y \geq y^*]$ of
 693 observing y_i given that $y_i \geq y^*$ is

$$\mathbb{P}[Y = y|Y \geq y^*] = \frac{\mathbb{P}[Y = y]}{\mathbb{P}[Y \geq y^*]} = \sqrt{\frac{2}{\pi}} \frac{e^{-\frac{(y-\mu)^2}{2\sigma^2}}}{\sigma \left[1 - \operatorname{erf}\left(\frac{y^* - \mu}{\sqrt{2}\sigma}\right)\right]}, \quad (25)$$

694 where $\operatorname{erf}(x) = \frac{2}{\sqrt{\pi}} \int_0^x e^{-\xi^2} d\xi$ is the Gauss error function. The log-likelihood $\mathcal{L}(\mu, \sigma, y^*)$ then verifies

$$-\frac{1}{N} \mathcal{L}(\mu, \sigma, y^*) = -\frac{1}{N} \sum_{i=1}^N \ln \mathbb{P}[Y = y_i|Y \geq y^*] = \ln(\sigma) + \ln \left[1 - \operatorname{erf}\left(\frac{y^* - \mu}{\sqrt{2}\sigma}\right)\right] + \frac{1}{2\sigma^2 N} \sum_{i=1}^N (y_i - \mu)^2, \quad (26)$$

695 up to irrelevant additive constants independent of the parameters μ and σ . For a given y^* , we minimize this
 696 quantity with respect to the parameters σ and μ to obtain $\hat{\sigma}(y^*)$ and $\hat{\mu}(y^*)$ and then chose y^* such that for
 697 any $y \geq y^*$ both $\hat{\sigma}(y)$ and $\hat{\mu}(y)$ are nearly constant (criterion (i) in Appendix 3.2). Finally, we obtain a lower
 698 bound on the uncertainty of the parameter values using the Fisher information matrix and the Cramer-Rao
 699 bound. To assess the quality of fit, we produce P-P plots comparing the cumulative distribution of data to

$$z = F(y|y^*) = \mathbb{P}[Y \geq y|Y \geq y^*] = \frac{\operatorname{erf}\left(\frac{y-\mu}{\sqrt{2}\sigma}\right) - \operatorname{erf}\left(\frac{y^*-\mu}{\sqrt{2}\sigma}\right)}{1 - \operatorname{erf}\left(\frac{y^*-\mu}{\sqrt{2}\sigma}\right)} \quad (27)$$

700 where z is the fraction of the data above $y \geq y^*$ according to the model, and Q-Q plots comparing the data
 701 to the inverse distribution function $y = F^{-1}(z|y^*)$.

702 *3.4. Normalization of μ across libraries*

703 The selection of a library L against a target T yields only the values of the highest selectivities $s(x)$ up
704 to an unknown multiplicative constant λ (see Box). The parameter $\sigma = \sigma_{L,T}$ is independent of λ but not
705 the parameter $\mu = \mu_{L,T}$. The relative values of $\mu_{L,T}$ for different libraries L selected against the same target
706 T are determined by performing selections where the different libraries are mixed in the initial population:
707 this leaves undetermined one overall multiplicative constant per target. Finally, we fix them by setting
708 $\mu_{\text{Germ},T} = 0$ for each target T . In practice, inferring μ from the tail of $P(s)$ is challenging, even more so
709 when different libraries are mixed, as one library often dominates the population after a few cycles. To
710 overcome this limitation, we can separately measure the selectivities of random sequences, which typically
711 belong to the mode of the distribution $P(s)$, located at $m = \mu - \sigma^2$.

712 For a given target, our approach is thus to first perform 3 cycles of selection with each library, Germ,
713 Lim and Bnab. Using the results from cycles 2 and 3, we estimate as many selectivities $s_{L,T}(x)$ as possible
714 (see Box and Fig. 1A). We then identify 2 to 4 sequences with largest selectivity from each library, which
715 we mix with 2 to 4 random sequences from each library, and perform one round of selection of the mixture
716 of these ~ 20 sequences. From the results of this experiment, we estimate with high precision the relative
717 selectivities of top and typical sequences from the different libraries (Fig. 1B). We typically find that the
718 random sequences from a same library have a similar selectivity which we use to define the relative modes
719 $m_{L,T}$ of the 3 libraries. Given these modes $m_{L,T}$, we then infer from the available values of $s_{L,T}(x)$ the
720 parameter $\sigma_{L,T}$ by maximum likelihood, using the relationship $\mu_{L,T} = m_{L,T} + \sigma_{L,T}^2$. Finally, we fix the
721 remaining overall multiplicative constant by setting $\mu_{\text{Germ},T} = 0$.

722 In practice, to reduce the total number of experiments, we performed the selection of the full libraries in
723 mixtures; as we verified with one target, the results are equivalent to those obtained from separate selections
724 (Fig. S8). We also found unnecessary to estimate the selectivities of typical sequences against all targets once
725 we understood that these values are not controlled by the target.

	Mix3 (rounds 2, 3)				Mix3 (rounds 3, 4)				separate		Mix21 or Mix24	
	σ	κ	μ	τ	σ	κ		τ	σ	κ	σ	κ
Germ	DNA1	1.50 ± 0.23	0.68 ± 0.12	0.00 ± 0.61	2.12 ± 0.27	1.38 ± 0.13	0.49 ± 0.11		1.27 ± 0.07	0.27 ± 0.14	1.07 ± 0.10	0.27 ± 0.11
	DNA2	1.16 ± 0.13	0.41 ± 0.11	0.00 ± 0.22	1.22 ± 0.17				1.16 ± 0.20	0.51 ± 0.23		
	prot1	1.44 ± 0.18	0.41 ± 0.20	0.00 ± 0.46	8.75 ± 2.07	1.13 ± 0.09	0.40 ± 0.13					
	prot2	1.50 ± 0.17	0.71 ± 0.12	0.00 ± 0.30	1.42 ± 0.19	1.07 ± 0.14	0.29 ± 0.13					
Lim	DNA1	1.40 ± 0.22	0.71 ± 0.27	0.00 ± 0.41	2.97 ± 0.88	N/A	N/A		0.98 ± 0.31	0.08 ± 0.34	N/A	N/A
	DNA2	1.31 ± 0.23	0.70 ± 0.24	0.00 ± 0.39	1.45 ± 0.38				N/A	N/A		
	prot1	0.56 ± 0.05	-0.68 ± 0.10	1.27 ± 0.06	4.40 ± 0.56							
	prot2	0.55 ± 0.04	-0.33 ± 0.06	0.93 ± 0.06	2.36 ± 0.22							
BnaB	DNA1	0.73 ± 0.18	0.01 ± 0.19	1.03 ± 0.33	2.74 ± 0.67	N/A	N/A		N/A	N/A	N/A	N/A
	DNA2	0.66 ± 0.13	-0.40 ± 0.24	0.05 ± 0.16	1.01 ± 0.33							
	prot1	1.13 ± 0.50	0.38 ± 0.22	0.33 ± 1.34	2.15 ± 0.60							
	prot2	0.97 ± 0.22	0.27 ± 0.23	0.12 ± 0.29	1.22 ± 0.37							
Chicken1 NurseShank1 Frog3 Frog3	DNA1	0.35 ± 0.08	-0.22 ± 0.08	2.24 ± 0.12	8.09 ± 1.29	0.50 ± 0.03	-0.09 ± 0.08		N/A	N/A	N/A	N/A
	DNA2	0.41 ± 0.06	-0.48 ± 0.14	2.07 ± 0.08	3.55 ± 0.74				N/A	N/A		
	prot1	0.45 ± 0.05	-0.52 ± 0.12	3.03 ± 0.07	21.98 ± 3.67	0.45 ± 0.05	0.31 ± 0.23					
	prot2	0.45 ± 0.05	-0.52 ± 0.12	1.51 ± 0.07	4.82 ± 0.80	0.57 ± 0.04	-0.05 ± 0.08					
Chickent1 NurseShank1 Frog3 Frog3	DNA1	0.67 ± 0.11	-0.41 ± 0.13	2.55 ± 0.14	16.00 ± 3.46				0.61 ± 0.13	-0.53 ± 0.19	0.64 ± 0.07	-0.56 ± 0.13
	PVP	0.59 ± 0.09	-0.17 ± 0.12	1.77 ± 0.12	5.63 ± 1.04				1.22 ± 0.45	0.52 ± 0.20	1.22 ± 0.45	0.52 ± 0.20
	DNA1											
PVP								0.04 ± 0.05	0.04 ± 0.05			

Table 1: Parameters obtained from fits of the distribution of selectivities to generalized Pareto distributions (κ, τ) and log-normal distributions (σ, μ) for experiments presented here and in our previous work [14]. N/A indicates that the data was insufficient to make a meaningful fit. For selectivities against the protein targets between rounds $c = 2$ and $c + 1 = 3$, values are given for two independent replica of the experiment. The given uncertainties correspond to a single standard deviation around the maximum likelihood estimate as given by the Cramer-Rao bound. In the case of Frog3 against DNA1, and only in this case, the value of κ differs from the one reported in our previous work [14] for reasons explained in Appendix 3.2 and Figure S15.

726

SUPPLEMENTARY FIGURES

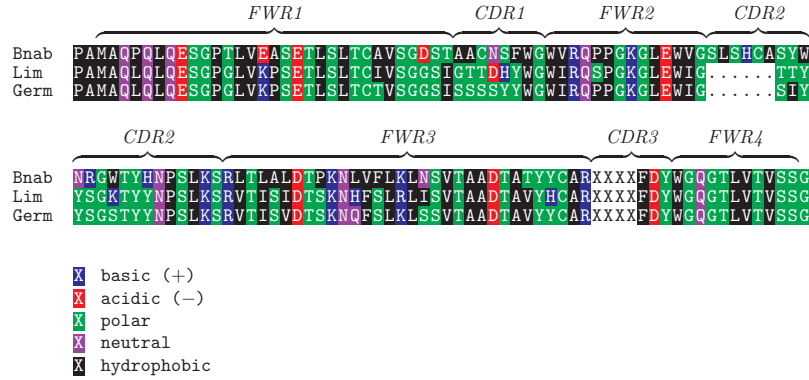


Figure S1: Alignment of the sequences of the three scaffolds, Bnab, Lim and Germ. The 4 randomized positions correspond to the part of the CDR3 indicated by XXXX.

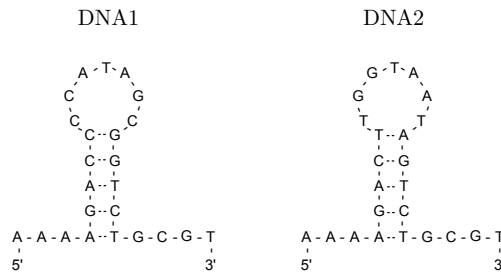


Figure S2: DNA1 and DNA2 binding targets. The targets display a hairpin structure at room temperature. They share a common stem sequence but the sequence of their loop differ. A biotin is placed at the 5' ends to allow for immobilization on streptavidin-coated magnetic beads.

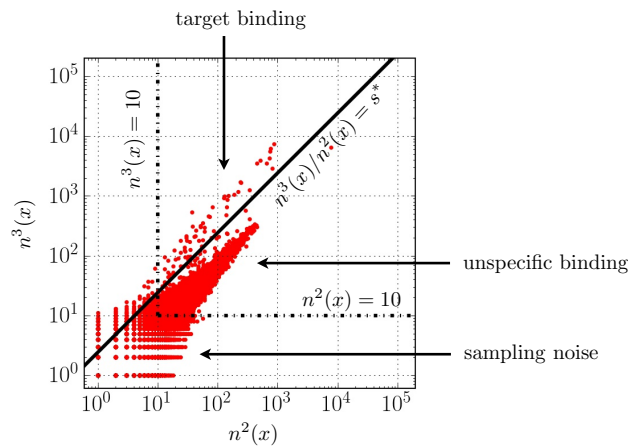


Figure S3: Illustration of the choice of the cutoff s^* below which measured selectivities are attributed to unspecific binding. The number $n^3(x)$ of counts in the sequencing data at round $c = 3$ is plotted against the number $n^2(x)$ of counts at round $c - 1 = 2$ for a selection of the Bnab library mixed with the two other libraries against the DNA1 target. An accumulation of sequences with similar selectivities is observed along the diagonal, with larger variance for smaller values as expected from an increased sampling noise. This is interpreted as arising from unspecific binding, associated with a selectivity s_{US} independent of the sequence. We define a cut-off s^* such that sequences x with $s = n^3(x)/n^2(x) \geq s^*$ cannot be attributed to unspecific binding. In addition, we restrict to sequences x with $n^2(x) \geq 10$ and $n^3(x) \geq 10$, as represented by the vertical and horizontal lines, to ensure that the inferred selectivities are not dominated by sampling noise.

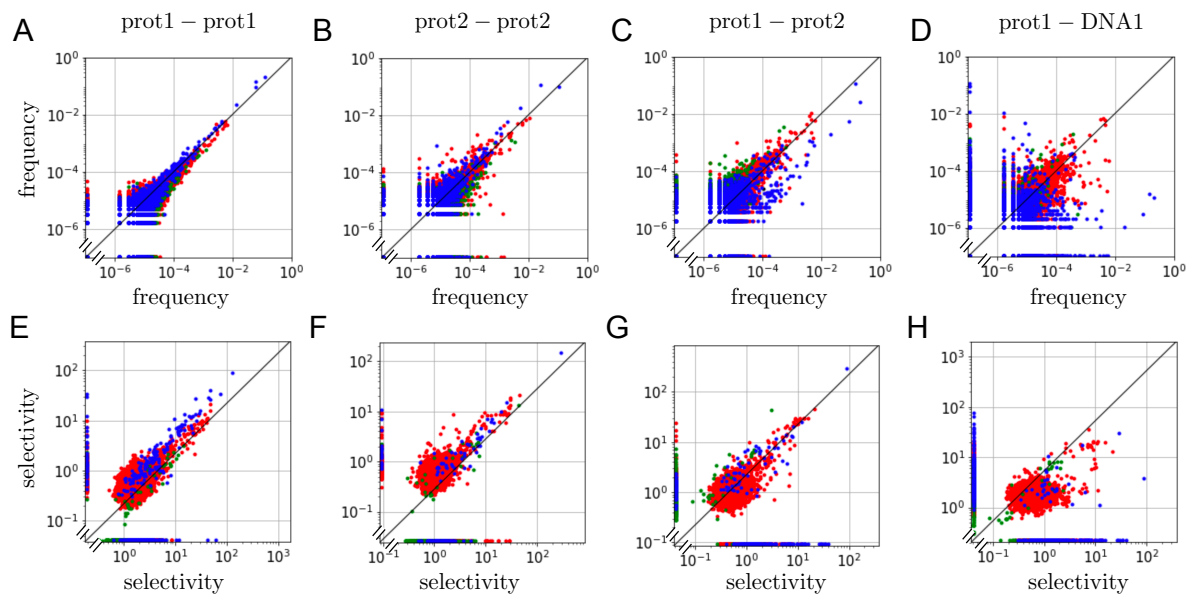


Figure S4: Comparisons between results of replicate and non-replicate experiments. **A.** Comparison of the frequencies $f^3(x) = n^3(x) / \sum_{x'} n^3(x')$ computed after the third cycle ($c = 3$) between two independent replicate experiments where a mixture of the Germ (in blue), Lim (in green) and Bnab (in red) libraries is selected against the protein target prot1. Due to stochastic sampling, some sequences x are well represented in one experiment ($n^3(x) \geq 10$) but not in the other; they are represented by the points along the two axes. As expected, the frequencies of the most prevalent sequences are the most reproducible. **B.** As in A but for protein target prot2. **C.** Comparing an experiment with prot1 as target with another with prot2 as target: common sequences are enriched in the two cases, although with not exactly the same frequencies. **D.** Comparing an experiment with prot1 as target with another with DNA1 as target, showing that different sequences are enriched in each case. In particular, the most frequent sequences when selecting against one target are absent in the third round when selecting against the other (points along the axes). **E, F, G, H.** Comparison of selectivities $s(x)$ calculated from the frequencies between the second and third rounds as $s(x) = \lambda n^3(x) / n^2(x)$. Points along the axes correspond to sequences for which the selectivity could be estimated only for one of the two experiments. We verify that in cases E, F, G where the targets are similar the same top selectivities are recovered (up to a multiplicative constant corresponding to a shift in log-log plots). Beyond stochastic effects, reproducibility is mainly limited by the differences in the production of the targets, as shown in Fig. S12.

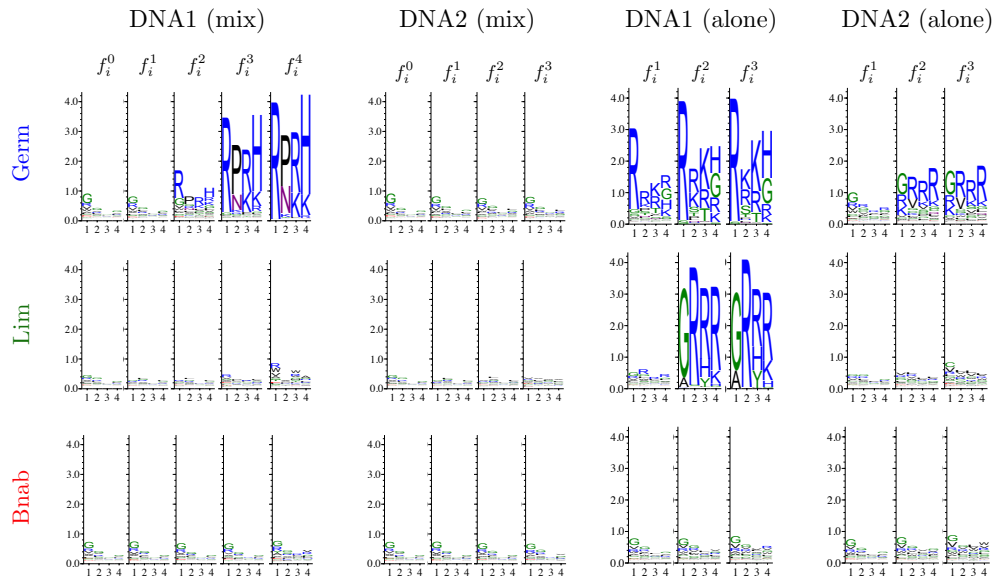


Figure S5: Extension of the figure in the Box to the 3 libraries Germ, Lim, Bnab selected either in a mixture (mix) or on their own (alone) against the DNA1 and DNA2 targets. The sequences logos represent the frequencies $f_i^c(a)$ of amino acids at each successive cycle $c = 0, 1, 2, 3, 4$.

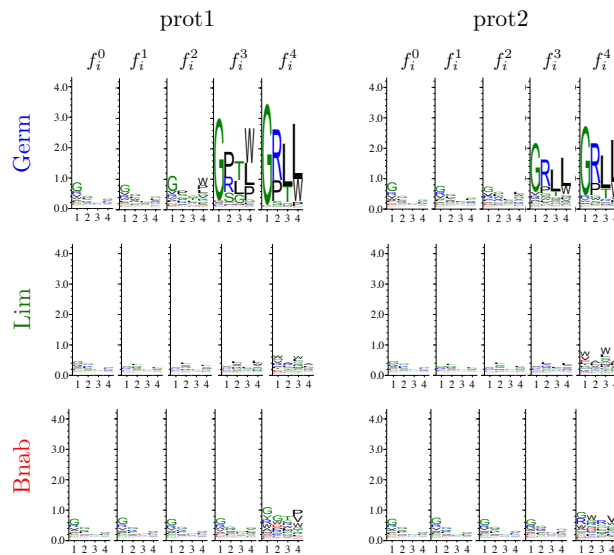


Figure S6: Extension of the figure in the Box to the 3 libraries Germ, Lim, Bnab selected in mixture against the prot1 and prot2 targets. The sequences logos represent the frequencies $f_i^c(a)$ of amino acids at each successive cycle $c = 0, 1, 2, 3, 4$.

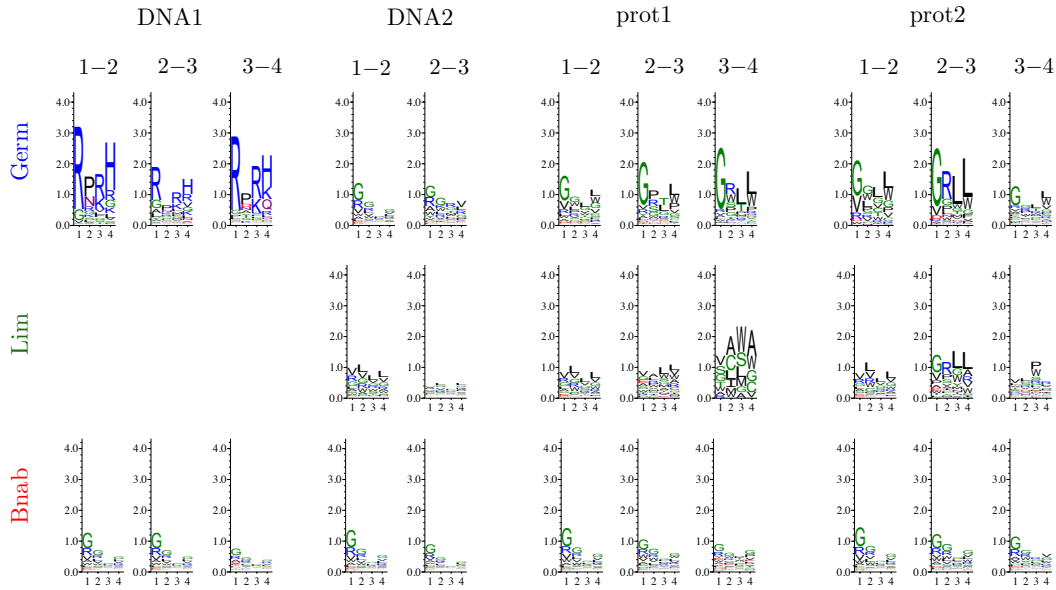


Figure S7: Sequence logos for the selectivities $\bar{s}(x)$ computed between two successive rounds (1-2, 2-3 or 3-4). The differences between rounds reflect sampling fluctuations.

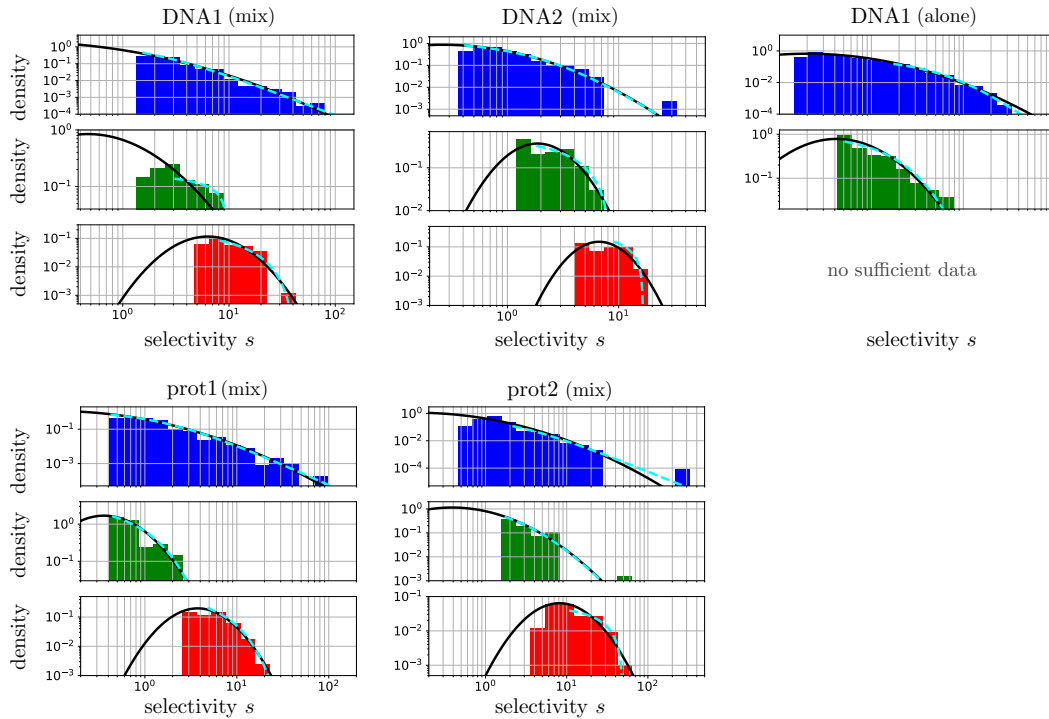


Figure S8: Distributions of selectivities of the three libraries (Germ in blue, Lim in green, Bnab in red) when selected either in a mixture (mix) or on their own (separate) against the different targets. This figure extends Fig. 1A that reports the selection against the DNA1 target of the Germ and Bnab libraries in mixture and of the Lim library on its own. In addition to the best fits to a log-normal distribution (black curves), the best fits to generalized Pareto distributions are also shown (cyan dotted curves). The selection of the Bnab library alone against the DNA1 target yielded insufficient data for a meaningful analysis.

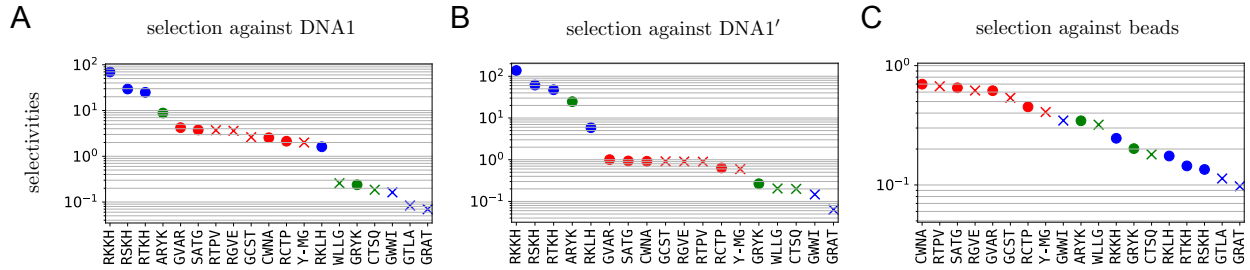


Figure S12: Supplementary experiments with minimal libraries. **A.** Selectivities of top and random sequences from the three libraries, Germ (in blue), Lim (in green) and Bnab (in red), against DNA1. This graph is identical to Fig. 1B. **B.** Results from a replicate experiment using a different stock of beads, showing that the selectivities are reproduced except for the Bnab sequences (in red), which have a systematically higher selectivity. **C.** Similar to A, but when selecting for binding to the beads in absence of the DNA1 target. The top selectivities are from the Bnab sequences (in red), indicating that they bind to the beads, a finding consistent with the discrepancy between A and B. Here, the differences in selectivities are also coming from differences of selectivity during amplification (Fig. S11). Consistent with Fig. S11, the top Germ sequences (blue dots) have in absence of the DNA1 target the worst selectivities.

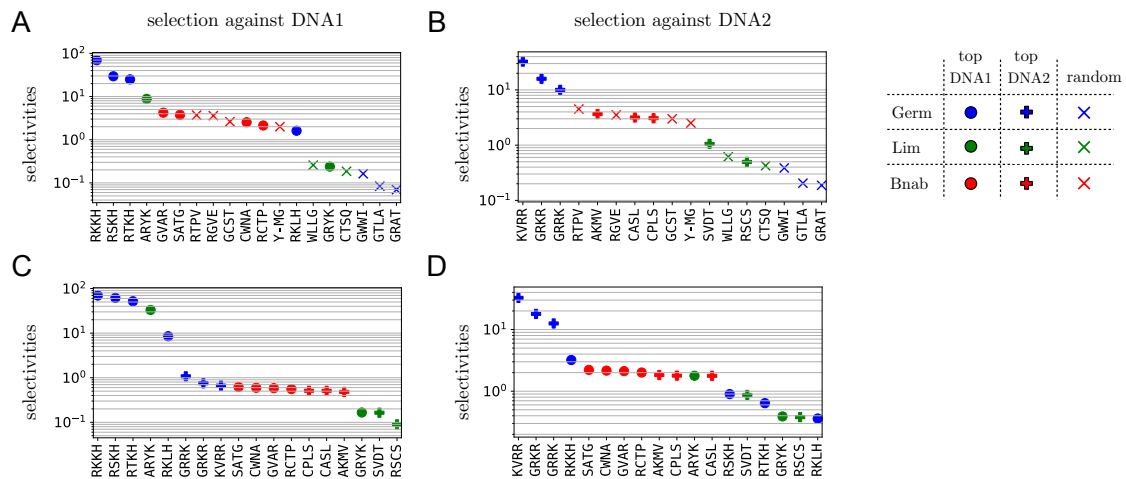


Figure S13: Cross selections with minimal libraries consisting of mixtures of top sequences against the DNA1 target (full circles) and top sequences against the DNA2 target (full crosses). **A,C.** Selection against the DNA1 target (same as Fig. 1B). **B,D.** Selection against the DNA2 target. The results confirm that some sequences from the Germ and Lim libraries bind specifically to the DNA1 target (blue dots and one of the green dots) and some sequences from the Germ library to the DNA2 target (blue crosses).

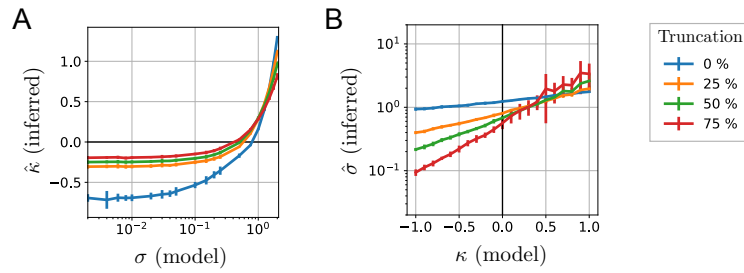


Figure S14: Relation between the parameter σ from log-normal fits and the parameter κ_N from generalized Pareto fits from numerical simulations. **A.** $N = 10^4$ values were drawn from a log-normal distribution with parameters $\mu = 0$ and varying σ (x-axis). The largest 25, 50, 75, 100 % of these values (i.e., 75, 50, 25, 0 % truncation) were fitted to a Pareto model with parameters κ and τ . The plot shows the estimation $\hat{\kappa}$ as a function of σ . Averages and standard deviations are taken over 25 independent realizations of the numerical experiment. It shows that limited sampling may cause a $\hat{\kappa} < 0$ to be inferred from values drawn from a log-normal distribution when σ is small, here $\sigma < 0.5$. **B.** Inverse simulation: A truncated log-normal model is fitted to the largest 25, 50, 75, 100 % among 500 values (i.e., 75, 50, 25, 0 % truncation) drawn from a Pareto model with parameters $\tau = 0.115$, $s^* = 0.001$ and varying κ (x-axis).

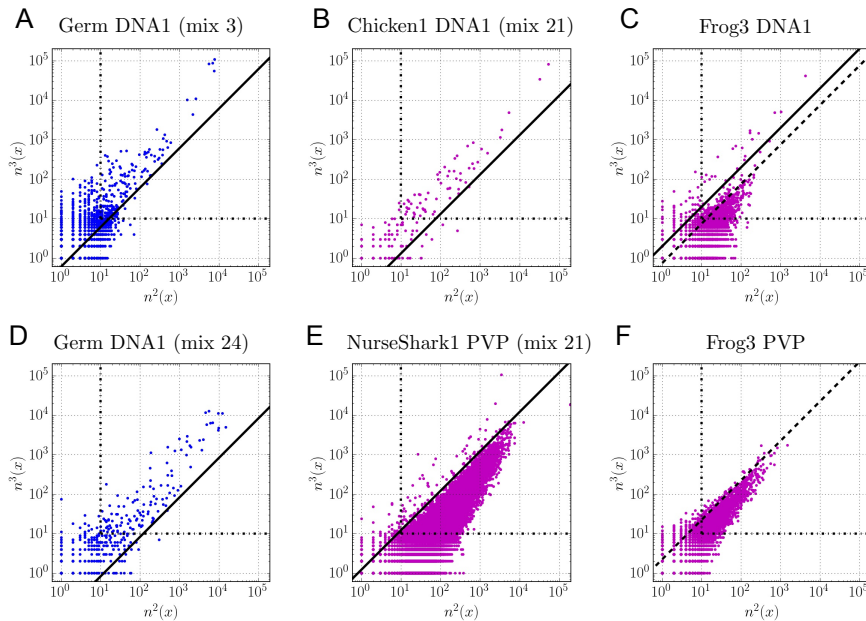


Figure S15: Definition of the threshold s^* above which selectivities s are considered for the experimental results reported here (A) and in Ref. [14] (B-F). As in Figure S3, the definition is based on a comparison between counts at the 2nd and 3rd cycles. The horizontal and vertical lines correspond to the criteria $n^2(x) \geq 10$ and $n^3(x) \geq 10$. The plain oblique line corresponds to the definition of s^* in this work. In the case of the selection of the Frog3 library against the DNA1 target, it differs from the value of s^* used in our previous work [14] (dotted oblique line) which failed to discard many selectivities coming from unspecific binding. In the case of the selection of the Frog3 library against the PVP target, all measured selectivities may be attributed to unspecific binding and we are therefore not including the inferred values of σ and κ in Fig. 4.

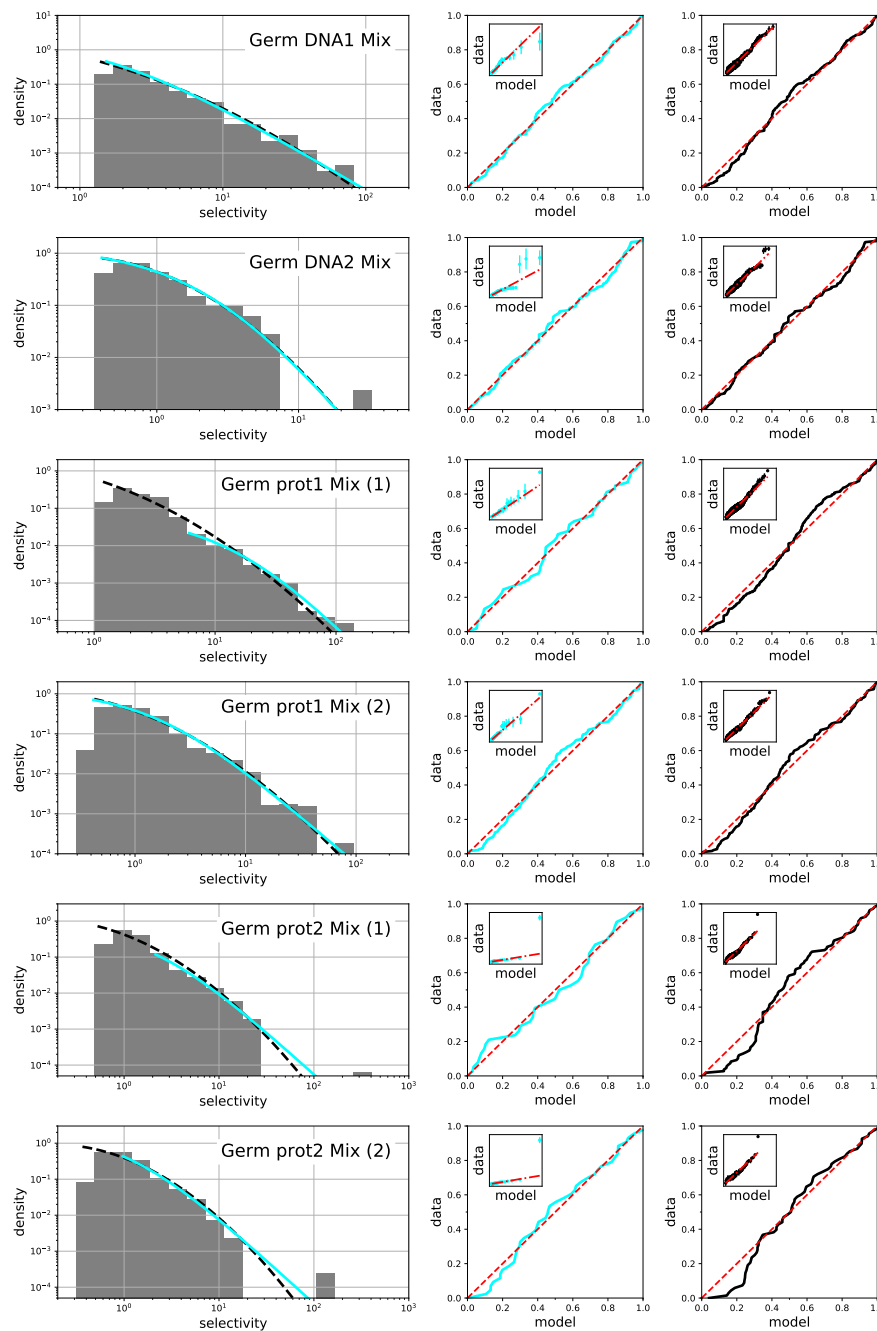


Figure S16: Assessments of the qualities of the fits of the selectivities to generalized Pareto distributions (cyan) and to log-normal distributions (black) for selections of the Germ library. The different graphs correspond to selections against different targets. For the protein targets prot1 and prot2, results from two replicate experiments are presented. All selectivities are computed by comparing the frequencies at the 2nd and 3rd cycle. The graphs on the right show the P-P and Q-Q (inset) plots for each fit. Perfect fits would correspond to the red dotted lines.

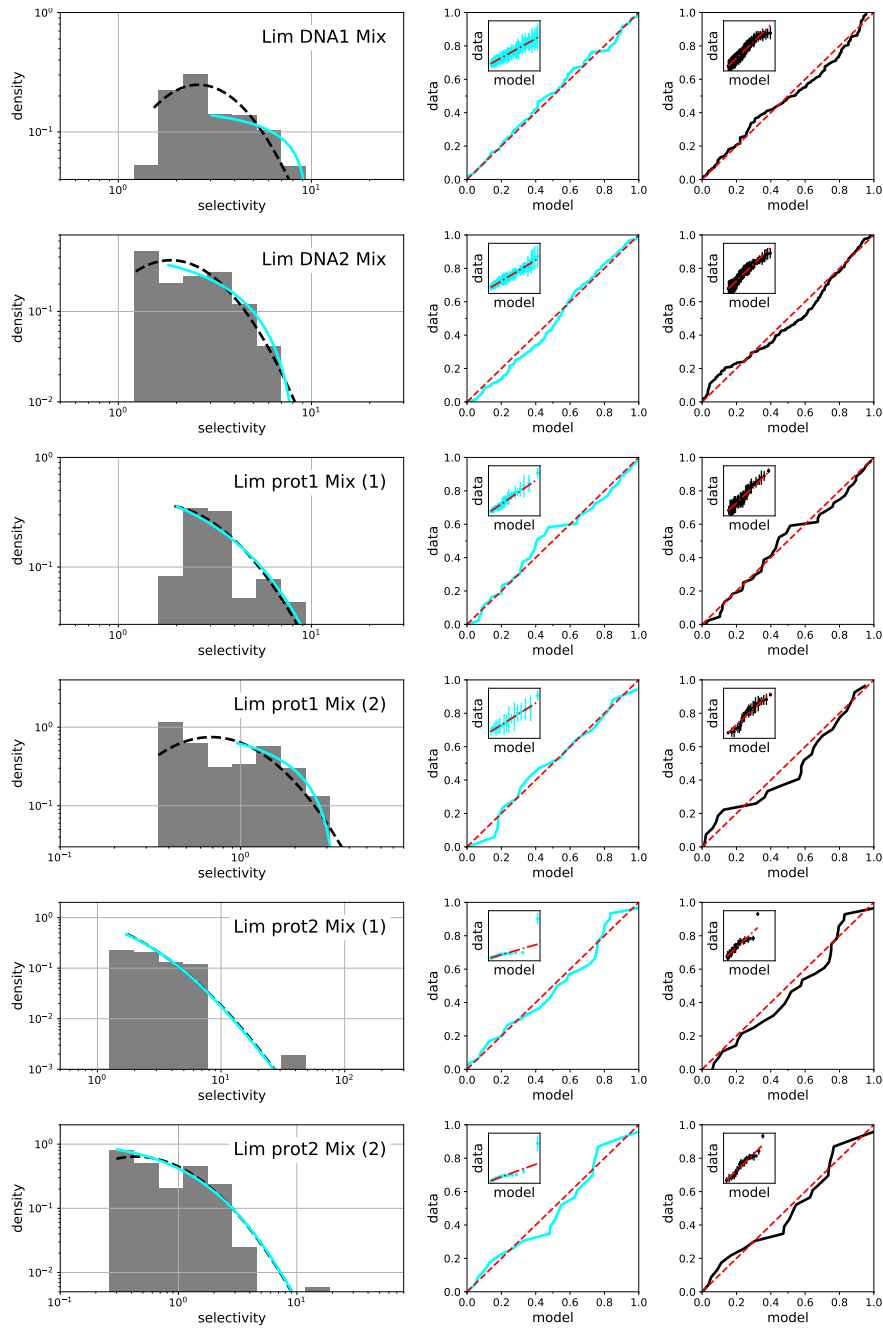


Figure S17: Same as Fig. S16 but for the Lim library instead of the Germ library.

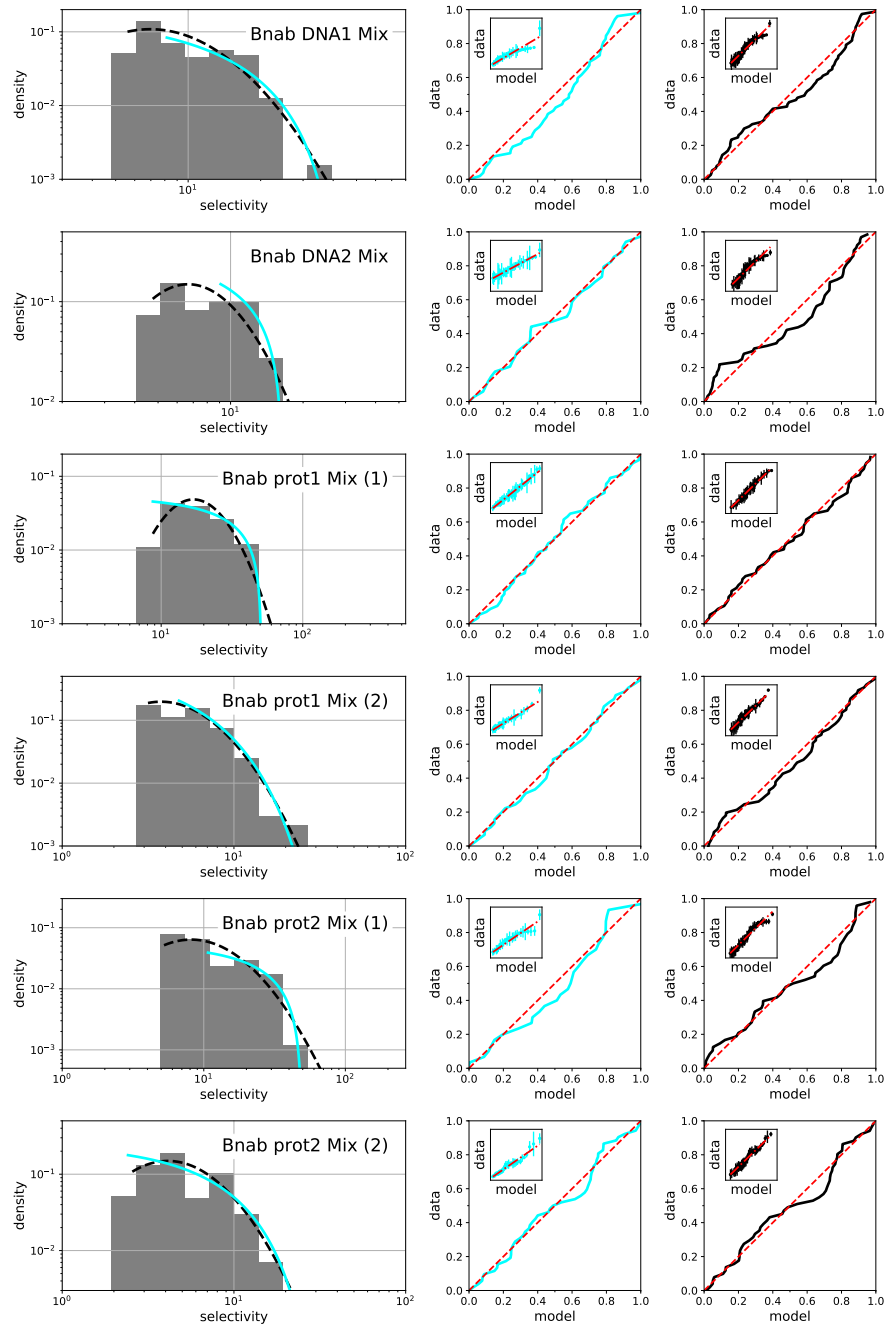


Figure S18: Same as Fig. S16 but for the Bnab library instead of the Germ library.

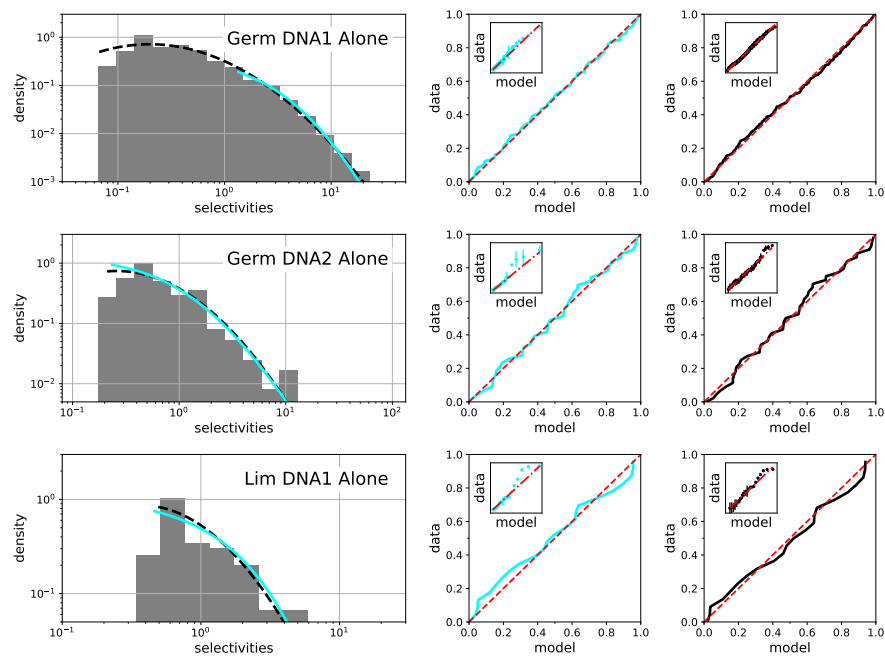


Figure S19: Same as Fig. S16 for the Germ library selected in isolation rather in a mixture with the two other libraries.

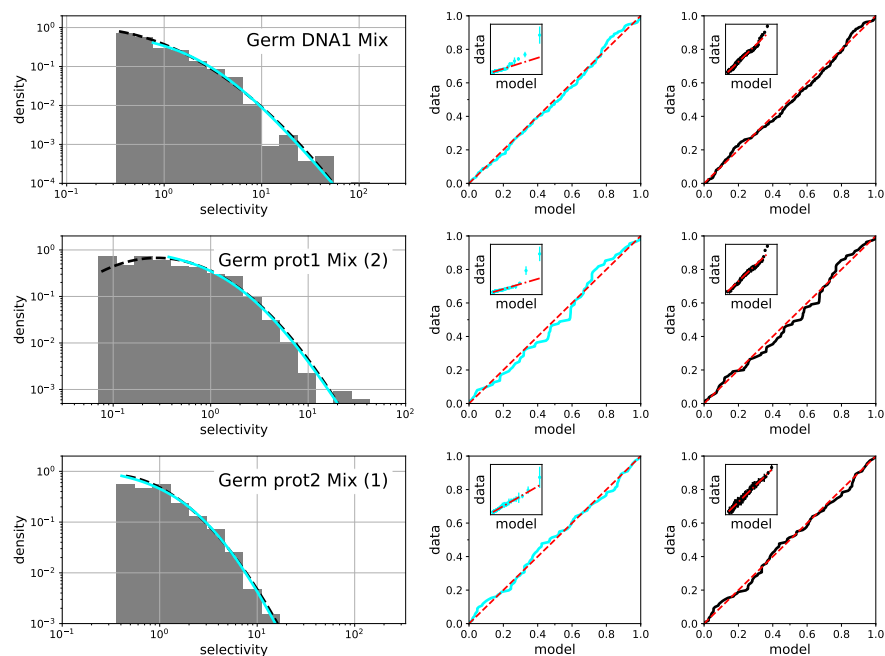


Figure S20: Same as Fig. S16 but for selectivities computed from a comparison between the 3rd and 4th cycle instead of the 2nd and 3rd cycle.

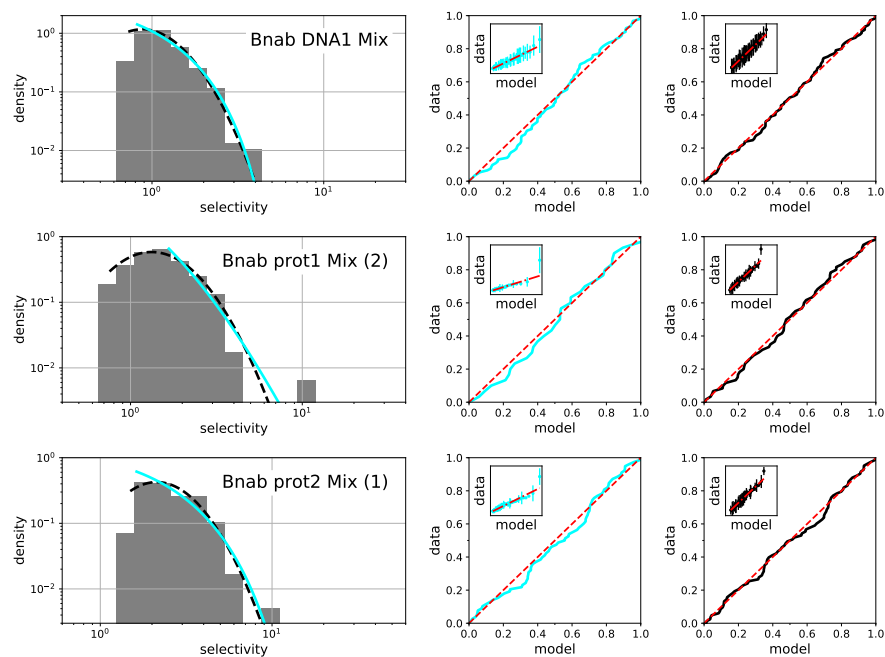


Figure S21: Same as Fig. S20 (selectivities computed from a comparison between the 3rd and 4th cycle) but for the Bnab library instead of the Germ library.

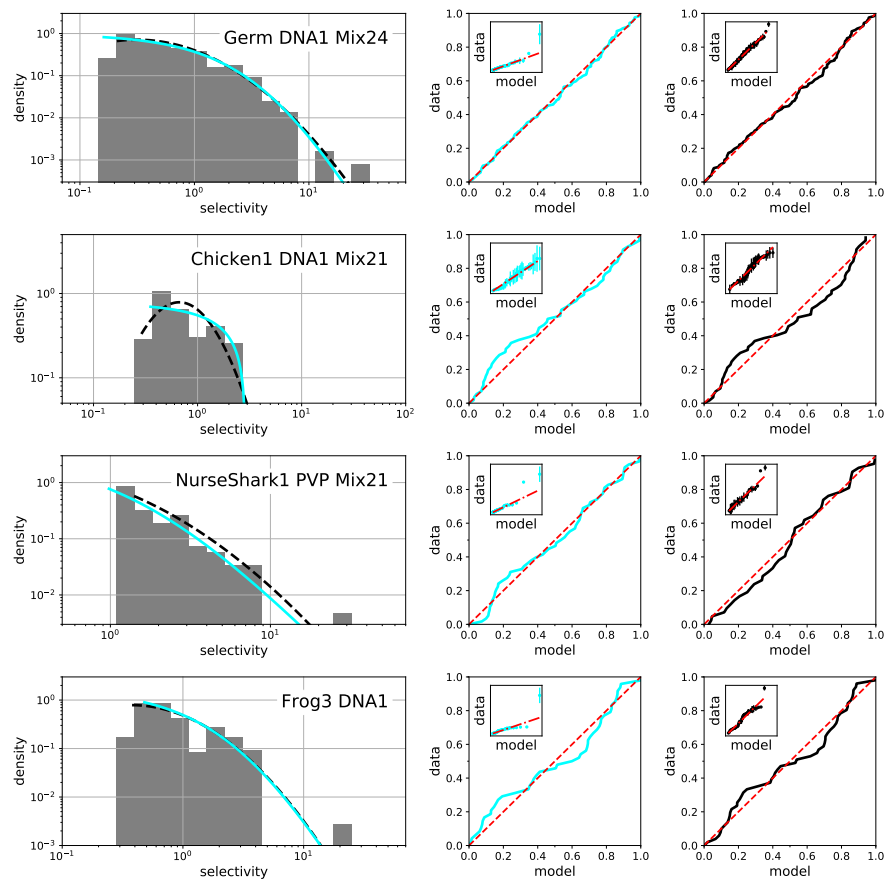


Figure S22: Same as Fig. S20 but for the experimental results reported in Ref. [14].